THE UNIVERSITY OF MICHIGAN

COLLEGE OF ENGINEERING

Nuclear Engineering Department

Laboratory For Fluid Flow and Heat Transport Phenomena

Technical Report No. 8

DETAILED INVESTIGATION OF CAVITATION PITTING CHARACTERISTICS FROM CAVITATING VENTURI TESTS

Lawrence L. Barinka

Frederick G. Hammitt

ORA Project 03424

under contract with:

NATIONAL AERONAUTICS AND SPACE ADMINISTRATION

CONTRACT NO. NAw-6550

WASHINGTON, D.C.

administered through:

OFFICE OF RESEARCH ADMINISTRATION ANN ARBOR

April 1963

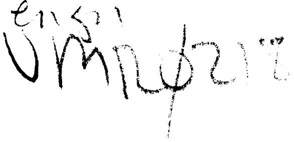

ABSTRACT

Empirical equations are developed to evaluate the cavitation damage parameters of weight loss, mean depth of penetration, and percent damaged area, for damage to only the polished surface and for the entire samples as tested in the venturi cavitation damage facility at the University of Michigan.

Quantitative results are presented of the contour of the cavitation pitting produced in mercury and comparisons are made between damage produced by water and mercury in the venturi damage facility.

ACKNOWLEDGMENTS

The authors wish to thank the Micrometrical Manufacturing Company of Ann Arbor for the loan of their Linear Proficorder, and Mr. David Calhoun of their company for his assistance in its operation.

Sincere thanks are also extended to the University of Michigan's Mechanical Engineering Department for the loan of their metallurgical microscopes, the Chemical and Metallurgical Engineering Department for the loan of their Research Metallographic camera, and to the Department of Naval Architecture and Marine Engineering for the loan of their integrating-planimeter.

Thanks is also given to Mr. H.M. Ring, research assistant in the Nuclear Engineering Department, for his assistance in checking the numerical calculations in this report.

TABLE OF CONTENTS

TABLE OF CONTENTS(continued)

LIST OF FIGURES

LIST OF FIGURES(continued)

LIST OF TABLES

IN APPENDIX

NOMENCLATURE

D : Actual diameter of pit crater

D_P: Visual diameter of pit crater

L : Actual characteristic length of irregular-shaped cavitation pits

L_P: Visual characteristic length of irregular-shaped cavitation pits

D': Actual distance between ridge peaks of a pit

h_m: Maximum ridge height

H_m: Maximum crater depth

v_R: Ridge volume of a pit

v_C: Crater volume of a pit

v_L: Volume loss per pit

K_P: Constant relating D and D_P

K : Constant relating volume loss of a pit, i.e., v_L, to D^3

K_S: Constant relating pitting rate on sides of a sample to pitting rate on polished surface

D_{RMC_i}: Root mean cube diameter for each of the 4 pit size categories, $i = 1,2,3,4$

C_i: $C_i = D^3_{RMC_i}$

D_{RMS_i}: Root mean square diameter for each of the 4 pit size categories, $i = 1,2,3,4$

S_i: $S_i = D^2_{RMS_i}$

n_i: Total number of pits in pit size category i on the polished surface of a sample, i = 1,2,3,4

n : Total number of pits on the polished surface of a test sample, $n = n_1 + n_2 + n_3 + n_4$

A_{PS}: Area of the polished surface of a test sample

A_T: Total area of a test sample exposed to cavitation

ρ: Density of test sample material

VL', WL', MDP', PDA': Volume loss, weight loss, mean depth of penetration, and percent damaged area, respectively, due to the damage on only the polished surface of a test sample

VL, WL, MDP, PDA: Volume loss, weight loss, mean depth of penetration, and percent damaged area, respectively, for an entire test sample

1.0 INTRODUCTION

The primary object of the work reported in this paper was the development of a group of equations to evaluate such cavitation damage parameters as weight loss, mean depth of penetration, and percent damaged area, for samples tested in the venturi cavitation damage facility of the University of Michigan's Nuclear Engineering Department. The equations were developed in such a manner that they could be evaluated from only a knowledge of:

(1) the number and size of cavitation pits occurring on the polished surface of a test sample, and

(2) some constant terms to be determined experimentally from individual pit profiles, pit size distributions, and rates of pitting.

A secondary, but very important object of the work reported herein was to gather as much information as possible about the general shape of the cavitation pits obtained on the materials tested in the venturi cavitation damage test facility.

TEST FACILITY. The test facility, mode of testing, and sample geometry have been previously discussed[6,7]*. How-

*Numbers in parenthesis refer to references at end of report.

ever, those details which are pertinent to the present report are repeated here for convenience.

The test facility (Figure 1) consists of a closed loop through which the cavitating fluid is circulated by a centrifugal pump. The loop includes a plexiglas venturi test section (Figure 2) that has a 6° included angle nozzle and diffuser, separated by a cylindrical throat of 0.51-in. diameter and 2.35-in. length. A cavitation field is produced that originates at the end of the cylindrical throat and which can be caused to visually terminate at any point along the diffuser. Set cavitation conditions (Visible Initiation, Standard, etc.), according to various termination points of the cavitation field, are indicated on Figure 2.

Two damage specimens are inserted in the cavitation field through the wall of the venturi as shown in Figure 2. The sample geometry is shown in Figures 3 and 4. The "polished surface" of a test specimen has a very highly polished finish of about 2 microinches (rms). The sides of a test specimen have a rougher machined finish of about 20 to 25 microinches (rms). Although the sides receive considerable damage, for reasons of time required, detailed observations are only made of the "polished surface".

BACKGROUND INFORMATION. The material necessary to begin the research reported herein was obtained from a previous project report by Walsh[18]. Walsh traced the surface of three stainless steel samples, which had been tested in

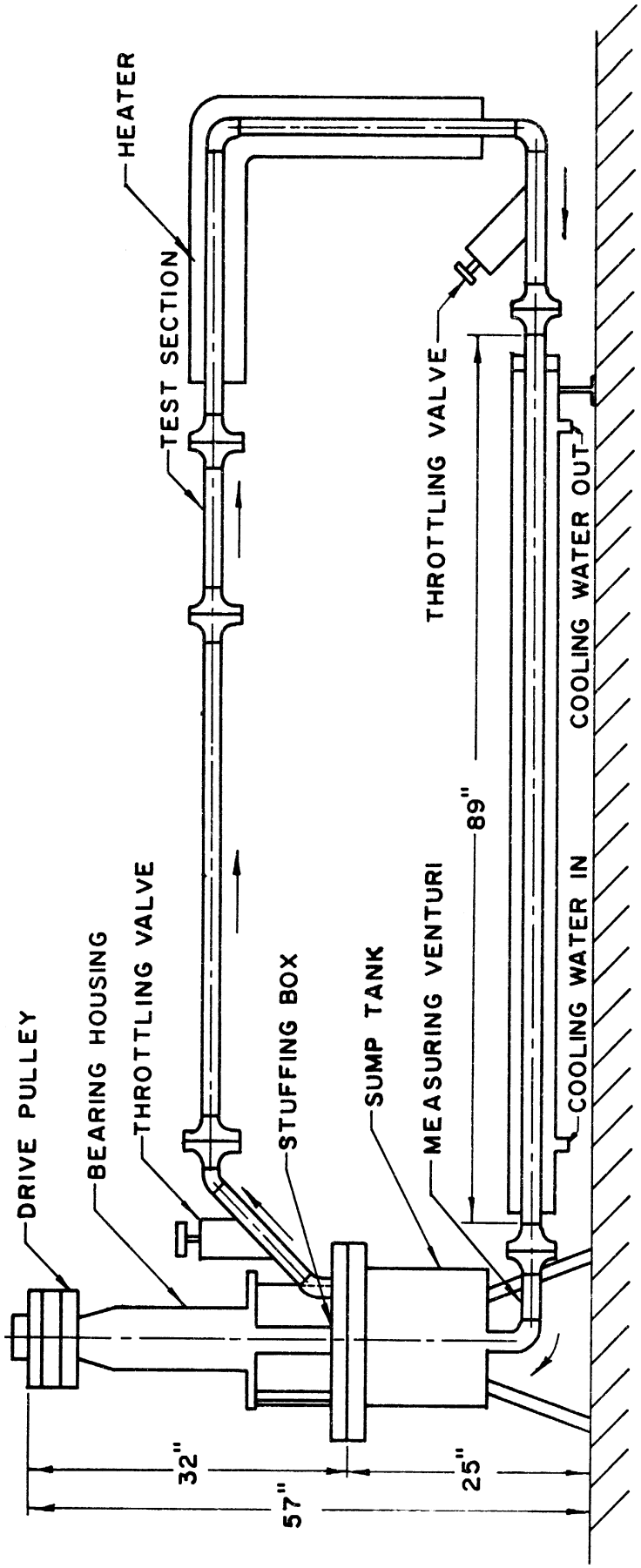

Figure 1. Schematic drawing of test facility.

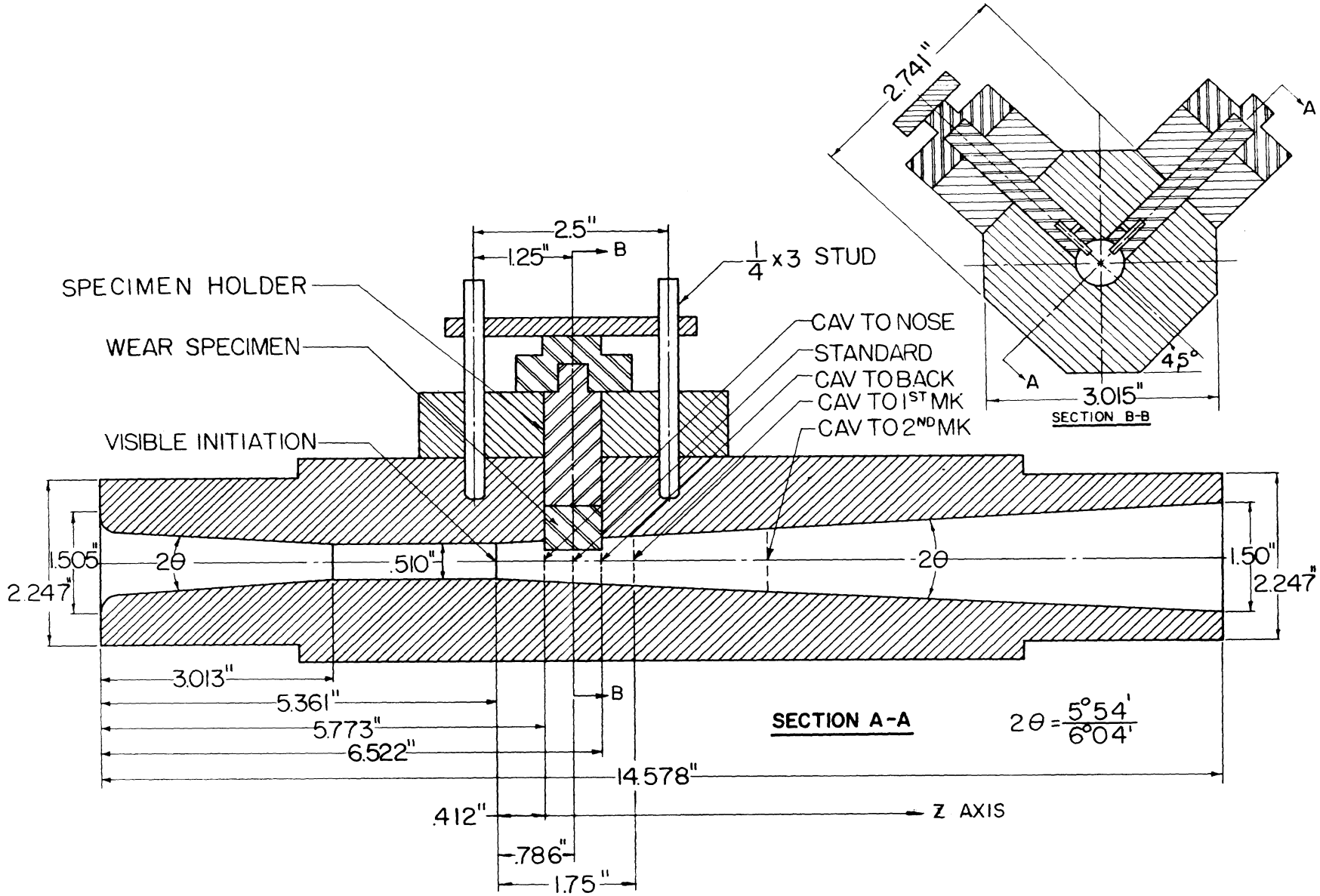

Figure 2. Cavitating venturi test section. The dotted lines in the diffuser represent the visual termination of the cavitation field for the various cavitation conditions shown.

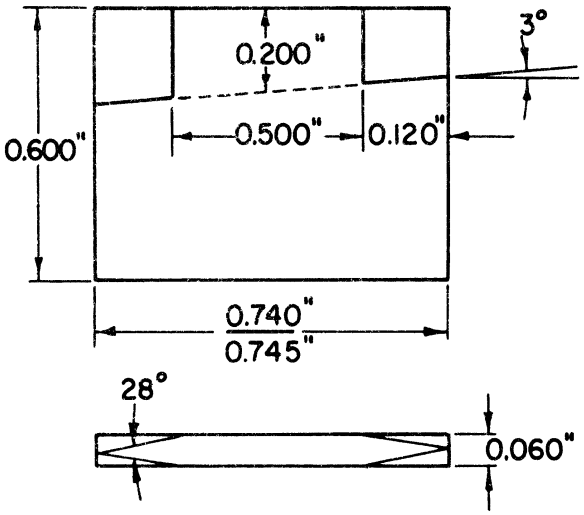

Figure 3. Schematic drawing of test specimen.

Figure 4. Macrograph of test specimen. The upper shadowed surface is the polished surface.

the cavitation facility with water as the cavitating fluid, with a linear proficorder*. He assumed the shape of a cavitation pit to be as shown in Figure 5, and for purposes of calculating the weight loss of a sample, he assumed the general shape of Figure 6. From the proficorder traces he tabulated the values of H_m, h_m, D, D_p, d, and then estimated h_{av} and H_{av}. According to his results, the relations between these parameters are best expressed as shown in Table I.

TABLE I

WALSH CAVITATION PIT PROFILE PARAMETERS

$H_m = (1/13)D$	$H_{av} = (2/3)H_m$
$h_m = 0.54\ H_m$	$h_{av} = (1/3)h_m$
$d = 0.56\ D$	$D_p = (5/4)D$

With these values and the assumed pit shape of Figure 6, Walsh proceeded to calculate the volume of material above and below the initial surface, in terms of D^3, and then assumed the volume loss per pit to be equal to the difference between the volume below and above the initial surface. He then obtained the weight loss per pit by merely multiplying the volume loss by the sample density. Summing the weight losses of each pit over an entire sample then gave the total weight loss of the sample. Walsh subdivided the pits into

*A linear proficorder is a mechanical-electronic instrument which provides a very precise, permanent, magnified chart of the surface contour over which it traces.

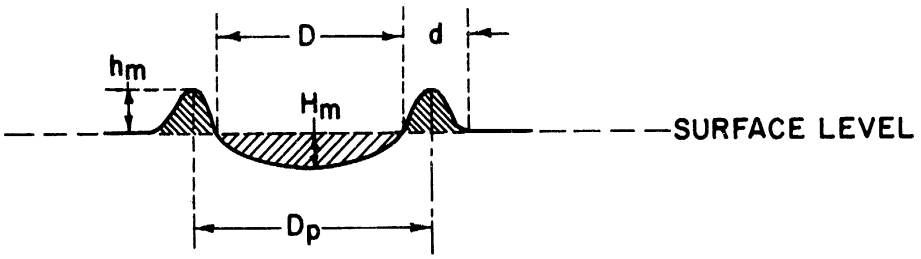

Figure 5. Walsh model of cavitation pit.

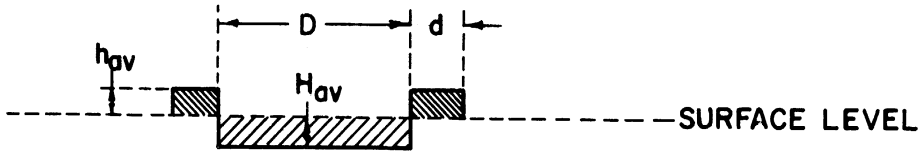

Figure 6. Walsh simplified model of cavitation pit.

three size ranges and found an average value of pit diameter for each range, which then allowed the evaluation of the weight loss of a sample from the product of the average pit diameter and number of pits for each pit size range.

MOTIVATION FOR INVESTIGATION. A discrepancy was found between the results predicted by Walsh's equation and actual weight loss measurements from an irradiated tracer test [6,7,17]. Because of this discrepancy and the fact that Walsh's work was based on the limited amount of damage test data available at that time, a more detailed study was desireable. It would also be meaningful to obtain empirical relations for Mean Depth of Penetration (i.e., volume loss per unit area) and Percent Damaged Area of a test specimen in addition to a Weight Loss equation, and to determine whether the pitting produced when water is the cavitating fluid (as was the case for Walsh's work) is similar to the pitting obtained for mercury as the cavitating fluid (from which the majority of the present data is drawn). For these reasons, the investigations reported herein were undertaken.

In the following sections, the desired equations are developed; the experimental results are summarized and discussed, and applied to determine suitable values for the empirical constants of the derived equations to put them into a working form; sample calculations are made with the equations and some restrictions are placed on their use.

2.0 DERIVATION OF EQUATIONS

In this section, six equations will be derived, three to determine the weight loss, mean depth of penetration and percent damaged area due to damage to only the polished surface of a cavitation damage specimen, and three to determine the total values of weight loss, mean depth of penetration, and percent damaged area of a damage specimen.

The primary object will be to develop all six equations in such a manner that they may be evaluated from only a knowledge of the number and size of pits occurring on the polished surface of a test sample.

2.1 Weight Loss

Consider first a single cavitation pit, with the following detailed symbol definitions:

D : Actual pit diameter as measured along the initial reference surface of a sample.

D_P: Pit diameter as seen visually thru a microscope or from a photograph.

v_C: Crater volume of a pit, i.e., volume of the pit below the initial reference surface.

v_R: Ridge volume of a pit, i.e., volume of the pit above the initial reference surface.

v_L: Actual volume loss per pit.

McHugh[11] made a detailed study of artificial pits made with a hardness indenter, and found that the volume of material raised above the initial reference surface, i.e., ridge volume, was equal to the volume of material displaced from below the initial reference surface, i.e., crater volume. Thus we can conclude that the materials tested, which were the same as the cavitation sample materials, are essentially incompressible under this type of deformation. It can also be concluded that for cavitation pits, if there is an actual metal removal from the sample, it must be equal to the difference between the crater and ridge volumes of a pit, i.e.:

$$V_L = V_C - V_R \qquad (2.1\text{-}1)$$

It is assumed to simplify the following derivation that all cavitation pits are approximately geometrically similar. Thus the volume loss per pit can be expressed in terms of the cube of a single characteristic dimension, in this case the actual pit diameter, D. Thus:

$$V_L \propto D^3$$

or

$$V_L = KD^3$$

where K is a constant to be determined experimentally.

From past experience, it is known that the pit diameter as seen visually through a microscope, D_P, differs from the actual pit diameter, D(which can be determined from a proficorder trace). Thus:

$$D = K_P D_P \qquad (2.1\text{-}2)$$

where K_P is also a constant to be determined experimentally.

The volume loss per pit now becomes:

$$v_L = K(K_P D_P)^3$$

or
$$v_L = KK_P^3 D_P^3 \qquad (2.1\text{-}3)$$

Next, consider n pits on the polished surface of a test sample. The volume loss due to these n pits is:

$$VL' = \sum_{i=1}^{n} v_{L_i} = \sum_{i=1}^{n} (KK_P^3 D_P^3)_i$$

or
$$VL' = KK_P^3 \sum_{i=1}^{n} D_{P_i}^3 \qquad (2.1\text{-}4)$$

The n pits occurring on the polished surface of a sample are subdivided arbitrarily into four size categories, where the range of each category will be defined in section 3.3. To eliminate the necessity of computing $D_{P_i}^3$, for each individual pit, Walsh[18] suggested the computation of an experimentally determined root mean cube (RMC_i) pit diameter for each of the four pit size categories. Then summation $D_{P_i}^3$ can be evaluated from only a knowledge of the number of pits, n_i, in each pit size category. Thus:

$$\sum_{i=1}^{n} D_{P_i}^3 = n_1(D_{RMC_1}^3) + n_2(D_{RMC_2}^3) + n_3(D_{RMC_3}^3) + n_4(D_{RMC_4}^3)$$

Let $C_i = D_{RMC_i}^3$. Then the above equation becomes:

$$\sum_{i=1}^{n} D_{P_i}^3 = n_1C_1 + n_2C_2 + n_3C_3 + n_4C_4$$

The volume loss due to n pits on the polished surface of a sample thus becomes:

$$VL' = KK_P^3(n_1C_1 + n_2C_2 + n_3C_3 + n_4C_4) \qquad (2.1\text{-}5)$$

Since material is not only removed from the polish-

ed surface of a test sample, but also from the sides of the sample, to determine the total volume loss per sample from only a knowledge of the pitting on the polished surface requires an additional factor relating the intensity of pitting on the sides of a sample to that on the polished surface. Thus let:

> K_S be a constant, determined experimentally, which when multiplied times the number of pits occurring on the polished surface of a sample gives the total number of pits occurring on the entire sample.

The total volume loss per sample thus becomes:

$$VL = KK_P^3K_S(n_1C_1 + n_2C_2 + n_3C_3 + n_4C_4) \qquad (2.1\text{-}6)$$

To obtain the desired weight loss equations, it is necessary only to multiply the volume loss equations by the specimen density, ρ.

Thus from equation (2.1-5) the weight loss due to the pits occurring on the polished surface only is:

$$WL' = \rho VL'$$

or

$$WL' = \rho KK_P^3(n_1C_1 + n_2C_2 + n_3C_3 + n_4C_4) \qquad (2.1\text{-}7)$$

Similarly, from equation (2.1-6) the total weight loss of a damaged sample becomes:

$$WL = \rho KK_P^3K_S(n_1C_1 + n_2C_2 + n_3C_3 + n_4C_4). \qquad (2.1\text{-}8)$$

2.2 Mean Depth of Penetration

Equations for the mean depth of penetration (i.e., volume loss per unit area) considering only the polished

surface of a test sample (MDP'), and for an entire sample (MDP) can be obtained from the volume loss expressions developed in the previous section. The following symbols are now defined.

A_{PS}: Area of the polished surface of a standard damage specimen.

A_T : Total exposed area, i.e., polished surface and sides, of a damage specimen.

From equation (2.1-5), the mean depth of penetration, for damage to only the polished surface of a specimen, can be obtained by dividing the volume loss, VL', by the area of the polished surface:

$$MDP' = VL' / A_{PS}$$

or
$$MDP' = KK_P^3(n_1C_1 + n_2C_2 + n_3C_3 + n_4C_4) / A_{PS} \qquad (2.2\text{-}1)$$

Similarly, from equation (2.1-6), MDP can be obtained.

$$MDP = VL / A_T$$

or
$$MDP = KK_P^3K_S(n_1C_1 + n_2C_2 + n_3C_3 + n_4C_4) / A_T \qquad (2.2\text{-}2)$$

2.3 Percent Damaged Area

The percent damaged area of the polished surface of a test sample (PDA') is defined as the summation of the area of all the cavitation pits on the polished surface divided by the area of the polished surface. Thus PDA' is:

$$PDA' = \left[(\pi/4 \sum_{i=1}^{n} D_i^2) / A_{PS}\right] \times 100 \ \%$$

But from the previous derivation of the weight loss equations:

$$D = K_P D_P \qquad (2.1\text{-}2)$$

Thus PDA' becomes:

$$PDA' = (25\pi K_P^2 \sum_{i=1}^{n} D_{P_i}^2) / A_{PS} \quad \%$$

To eliminate the necessity of computing each individual $D_{P_i}^2$, an experimental root mean square (RMS) pit diameter is found for each of the four pit size categories. Thus:

$$\sum_{i=1}^{n} D_{P_i}^2 = n_1(D_{RMS_1}^2) + n_2(D_{RMS_2}^2) + n_3(D_{RMS_3}^2) + n_4(D_{RMS_4}^2)$$

Let $S_i = D_{RMS_i}^2$. Then the above equation becomes:

$$\sum_{i=1}^{n} D_{P_i}^2 = n_1S_1 + n_2S_2 + n_3S_3 + n_4S_4$$

Thus the percent damaged area of the polished surface of a test sample becomes:

$$PDA' = 25\pi K_P^2(n_1S_1 + n_2S_2 + n_3S_3 + n_4S_4) / A_{PS} \quad \% \qquad (2.3\text{-}1)$$

The equation for the total percent damaged area (PDA) of a test specimen can be obtained from the last expression by merely multiplying by the factor K_S relating the wear on the sides of a sample to the wear on the polished surface, and by dividing by the total exposed area A_T rather than the area of the polished surface. Thus PDA becomes:

$$PDA = 25\pi K_P^2 K_S(n_1S_1 + n_2S_2 + n_3S_3 + n_4S_4) / A_T \quad \% \qquad (2.3\text{-}2)$$

3.0 EXPERIMENTAL PROCEDURES & RESULTS

The following constants of the equations derived in the preceding sections were evaluated from the experimental data as described below: K_P, K, D_{RMC_i}, D_{RMS_i}, and K_S.

3.1 Determination of K_P

As previously mentioned the apparent, visual diameter of a pit, D_P, as seen through a microscope or from a photograph, differs from the actual pit diameter, D, which can be determined from a proficorder trace of the pit profile. This discrepancy has been observed not only for cavitation pits, but also for artificial pits produced by a hardness indenter. Thus both artificial and cavitation pits were examined to determine the relation between the visual and actual size of each.

To determine the relation between D_P and D for artificial pits, four hardness indenter pits were made on a piece of annealed austenitic-stainless steel(89 Rockwell B hardness). Their diameters were made to correspond roughly to that of cavitation pits of the largest pit size category. These "artificial" pits were traced with a linear proficorder and photographed. A comparison of the proficorder traces of the four artificial pits with their photo-

graphs indicated an average value of:

$D_p = 1.22D$ i.e., the visually determined diameter of the artificial pits was 1.22 times the actual pit diameter.

The data used to obtain the results reported in this section is given in Tables A-I and A-II of the Appendix.

From the proficorder traces of the artificial pits, the following average values were also found:

$D_p = 1.02D'$ i.e., the visual pit diameter of the artificial pits is 1.02 times greater than the distance between ridge peaks of the pits.

$D = 7.689H_m$ i.e., the actual diameter of the artificial pits is 7.689 times greater than their maximum depth.

$H_m = 7.397h_m$ i.e., the maximun depth of the artificial pits is 7.397 times greater than their maximum ridge height.

Of course, all cavitation pits occurring on the surface of tested samples are not circular in shape. For the tabulation of pits according to size, pit counting tables have been developed which convert the irregularly shaped pits into equivalent circular pits. Thus to determine a relation between the visual and actual size of a cavitation pit, since diameters were not always available, it was necessary to choose a characteristic length for each pit and compare this length, L_p, on the photograph with the corresponding length, L, from the proficorder trace. The characteristic length was chosen for each pit so that it could be identified, with certainty, on both the photograph and proficorder trace of

the pit, and so that it occurred on the proficorder trace from a given pit which contained the maximum values of characteristic length (L), depth (H_m), and ridge height (h_m).

An annealed, type 302 stainless steel, cavitation damaged sample was traced with a linear proficorder and photographed. Six typical pits were then examined to determine the relation between L_p and L. The following average value was found:

$L_p = 0.853L$ i.e., the visual characteristic length of the cavitation pits is 0.853 times their actual characteristic length*.

Thus for the cavitation damage equations derived in the preceding sections, the photographic constant, K_p, relating the visual pit size to the actual pit size is:

$$K_p = 1.172 \quad \text{i.e., } 1/0.853.$$

The following values identifying the profile of the cavitation pits were also found from the proficorder traces of the six cavitation pits traced:

$L = 18.0H_m$ to $46.1H_m$ i.e., the actual characteristic length of the cavitation pits is from 18.0 to 46.1 times as great as their maximum depth.

$H_m = 2.5h_m$ to $69.4h_m$ i.e., the maximum depth of the cavitation pits is from 2.5 to 69.4 times as great as their maximum ridge height.

Since the spread was too large to validate the calculation of

---

*Note that while $D_p = 1.22D$ for hardness indenter pits, $L_p = 0.853L$ for cavitation pits. This apparent discrepancy is discussed in Section 4.1.

an average, no average value was calculated for the ratios of L to H_m and H_m to h_m. Also, it is to be noted that for the cavitation pits, the ridge is not symetrical around the pit crater*, as for artificial pits, but in general exists only partially around the crater, and it was the maximum value of this partial ridge that was used as the value of h_m.

3.2 Determination of K

In section 2.1, it was shown that the volume loss for each cavitation pit is:

$$v_L = KK_P^3 D_P^3 \qquad (2.1\text{-}3)$$

In the preceding section it was shown that the "best" value for K_P is:

$$K_P = 1.172$$

Thus v_L becomes:

$$v_L = K(1.172)^3 D_P^3$$

In section 2.1, it was also shown that the volume loss per pit is:

$$v_L = v_C - v_R \qquad (2.1\text{-}1)$$

Equating the last two expressions for v_L gives:

$$v_L = v_C - v_R = K(1.172)^3 D_P^3$$

---

*Out of 14 pits examined, the ridge was highest on the downstream side in 6 cases, highest on the upstream side in 3 cases, and approximately equal in the remaining 5 cases.

or $$K = (v_C - v_R) / (1.172)^3 D_P^3$$

or $$K = 0.621(v_C - v_R) / D_P^3 \qquad (3.2\text{-}1)$$

Thus the volume loss constant, K, for any cavitation pit can be evaluated experimentally by determining D_P, v_C, and v_R for the pit. The visual pit diameter, D_P, of any pit can be determined from a photograph of the pit. Proficorder traces taken at a known constant increment across the contour of the pit can be used to determine the ridge and crater volumes, v_R and v_C, of the pit by applying the following method:

Consider first Figures 7 and 8. The areas a_C and a_R on each proficorder trace can be evaluated by using a planimeter to trace around the respective areas.

The volumes can then be found as follows:

$$a_{C_{i,i+1}} = (a_{C_i} + a_{C_{i+1}}) / 2$$

$$v_{C_{i,i+1}} = I a_{C_{i,i+1}}$$

$$v_C = \sum_{1,2}^{N-1,N} v_{C_{i,i+1}}$$

or $$v_C = I \sum_{1,2}^{N-1,N} a_{C_{i,i+1}}$$

Similarly: $$v_R = I \sum_{1,2}^{N-1,N} a_{R_{i,i+1}}$$

An annealed, type 302 stainless steel, cavitation damaged sample tested in mercury was traced with a linear

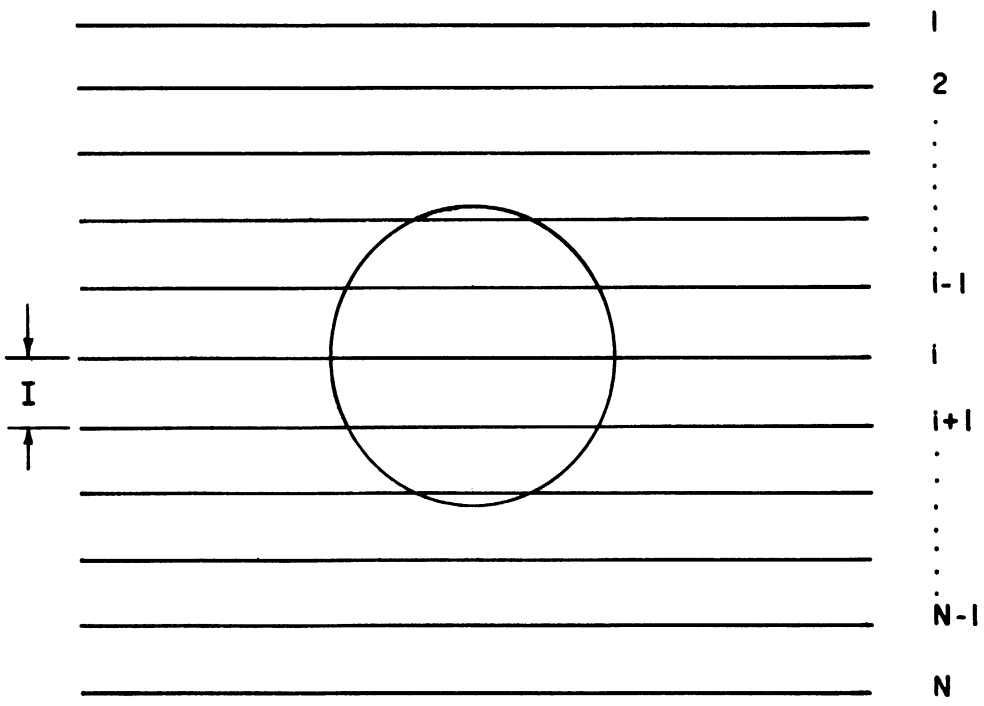

Figure 7. Schematic drawing of the paths of N proficorder traces at equal increments I across a cavitation pit. The circle represents the surface area damaged by the pit.

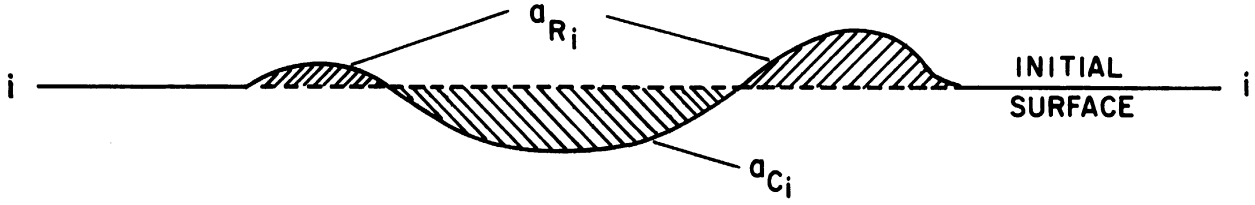

Figure 8. Schematic drawing of the profile of the cavitation pit in Figure 7 as shown by proficorder trace i.

proficorder (see Figures 9 and 10) and 14 typical pits were examined by the above technique to determine the volume loss proportionality constant, K, from equation (3.2-1). It was found that the average value of the volume loss constant for the 14 pits examined was:

$$K = 7.346 \times 10^{-3}$$

The data used to obtain the above result can be found in Tables A-III and A-IV of the Appendix.

An average value of v_R/v_C was also computed for the 14 pits examined and was found to be:

$$v_R / v_C = 0.328$$ i.e., the ridge volume is about one third of the volume of the crater of a typical cavitation pit.

Thus the actual average metal removal for the 14 pits examined was about two thirds of the volume of the craters of the pits. Of the 14 cavitation pits examined, 3 were approximately circular craters and 11 were of irregular contour. The ridge to crater volume ratios for both types are of the same order of magnitude.

3.3 Determination of D_{RMC_i} and D_{RMS_i}

For the present cavitation tests using mercury as the cavitating fluid, pits were observed that varied in size from about $0.1 \leqq D_p$, mils $\leqq 10.5$. All approximately circular pits are tabulated according to their diameter, and as previously mentioned, irregularly shaped pits are converted into equivalent circular pits according to the surface area

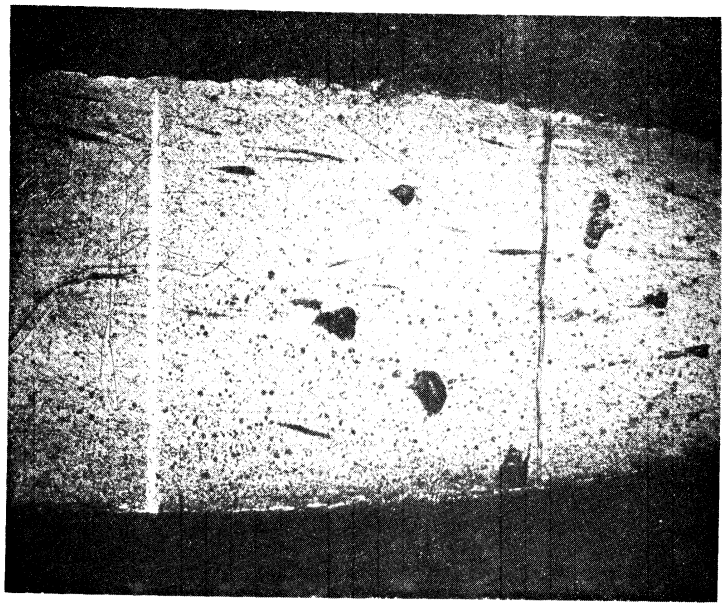

Figure 9. Macrograph of proficorder traced area 1. Stainless steel specimen #63. Cavitation to nose. Throat velocity-34 fps. 100 hours test duration in mercury. 37.5X. Flow is from left to right. The area between the scribed lines was traced from left to right at 0.001 inch increments across the specimen. The traced area is near the trailing edge of the specimen.

Figure 10. Macrograph of proficorder traced area 2. Same as Figure 9, except traced area is near the leading edge of the test specimen.

damaged. The equivalent diameters are then tabulated. To facilitate the pit counting of damaged samples, four pit size categories were selected with ranges as shown in Table II.

TABLE II

PIT SIZE CATEGORIES

Category	Size Range(mils)
1	$0.46^{*} \leqq D_{P_1} < 1.15$
2	$1.15 \leqq D_{P_2} < 2.76$
3	$2.76 \leqq D_{P_3} < 5.52$
4	$5.52 \leqq D_{P_4} \leqq 11.04$

These categories include all observed pits except those with visual pit diameters less than 0.46 mils, which in section 6.1, are shown to provide a neglegible contribution to weight loss. Thus considering these four categories: if n pits occur on the polished surface of a test sample, and if n_1 pits can be considered to be in pit size category 1, and n_2, n_3, and n_4 pits in pit size categories 2,3, and 4, respectively, then $n = n_1 + n_2 + n_3 + n_4$.

In section 2.1 (Eq.2.1-4), the volume loss due to n pits occurring on the polished surface of a test sample was shown to be proportional to the summation of the cube of the visual diameters of the n pits. As previously mentioned, to eliminate the necessity of computing each individual D_{Pi}^3, an experimental root mean cube (RMC) pit

*0.46 mils corresponds to 1 division on the scaled microscope eyepiece used in observing test samples.

diameter for each of the four pit size categories is to be determined. A similar substitution of an RMS constant was made in the derived equations for percent damaged area.

To determine the RMS and RMC diameters for each pit size category, eight typical damaged samples were observed under 100 power magnification. The four pit size categories were subdivided as shown in Table A-V of the Appendix, and the total number of pits on all eight samples in each of these subdivisions was determined. The total number of pits in each subdivision, n', was then multiplied by $D_{P_{av}}^2$ and $D_{P_{av}}^3$ as shown in Table A-VI. The products of each subdivision, $n'D_{P_{av}}^2$ and $n'D_{P_{av}}^3$, were then summed for each pit size category, and divided by the total number of pits in each category to give the RMS constant ($S_i = D_{RMS_i}^2$) and the RMC constant ($C_i = D_{RMC_i}^3$) as follows:

$$C_i = \frac{\sum(n'D_{P_{av}}^3)_i}{\sum n_i'}$$

and $$D_{RMC_i} = C_i^{.333}$$

Similarly:

$$S_i = \frac{\sum(n'D_{P_{av}}^2)_i}{\sum n_i'}$$

and $$D_{RMS_i} = S_i^{.500}$$

where i corresponds to the four pit size categories.

The results summarized in Table A-VII in the Ap-

pendix are listed below in Table III for convenience.

TABLE III

SUMMARY OF RMS & RMC CONSTANTS

Pit Size Category	Pit Size Range(Mils)	D_{Pav} (Mils)	D_{RMS_i} (Mils)	S_i (Mils^2)	D_{RMC_i} (Mils)	C_i (Mils^3)
1	0.46 - 1.15	0.805	0.805	0.6480	0.805	0.5216
2	1.15 - 2.76	1.955	1.776	3.1525	1.821	6.0363
3	2.76 - 5.52	4.140	4.060	16.4799	4.144	71.1547
4	5.52 -11.04	8.280	6.828	46.6233	6.941	334.4513

3.4 Determination of K_S

The samples used for cavitation tests extend into the fluid stream a mean distance of 0.2 inches from the wall of the venturi (see Figure 2). The end face of a typical sample (i.e., face approximately parallel to wall) is highly polished*, and constitutes about 11% of the total specimen area exposed to cavitation (see Figures 3 and 4). The sides of a typical sample, which constitute the remaining 89% of exposed area, are not polished and have only a machined finish**, upon which accurate pit counting, especially of the smaller pits, is difficult. For this reason, and to conserve labor, only the polished surface of a test sample is pit-counted. Since material is removed not only from the polished surface, but also from the sides, an expression

*Surface roughness usually about 2 microinches(rms).
**Surface roughness usually about 20 microinches (rms).

is needed to relate the damage on the sides of the sample to that on the polished surface. Specifically, an experimental constant, K_S, is desired such that when it is multiplied times the number of pits occurring on the polished surface of a test sample, the product gives the total number of pits occurring on the entire sample.

To determine the desired constant K_S, six samples were observed under 100 power magnification: two "water" samples and four "mercury" samples (including two special samples with their sides initially polished). The total number of pits in each size category on both the polished surface and sides of the samples was determined. The results are summarized in Table A-VIII in the Appendix. For all the samples observed, there were on the average 2.601 times as many pits, in all four pit size categories, on the sides of a sample as on the polished surface. Thus for n pits on the polished surface of a sample, there are 2.601 n pits on the sides, or 2.601 n + n = 3.601 n pits on the entire test sample. Thus:

$$K_S = 3.601$$

4.0 DISCUSSION OF RESULTS

4.1 Visual and Actual Pit Sizes

As previously mentioned, $D_P = 1.22D$ for artificial pits and $L_P = 0.853L$ for cavitation pits. To explain this apparent discrepancy, consider the models of artificial and cavitation pit contours shown in Figures 11 and 12, where parameter values tabulated from proficorder traces of the artificial and cavitation damaged samples will be used (Table IV).

TABLE IV

SUMMARY OF PIT PROFILE PARAMETERS

Artificial Pit	Cavitation Pit
$D_P = 1.22D$	$L_P = 0.853L$
$D_P = 1.02D'$	$L = 18.0H_m$ to $46.1H_m$
$D = 7.689H_m$	$H_m = 2.5h_m$ to $69.4h_m$
$H_m = 7.397h_m$	$L = 45h_m$ to $3199.3h_m$
$D = 56.876h_m$	

For both the camera and microscope used to observe and photograph cavitation and artificial-pit samples, the set-up is as shown schematically in Figure 13, i.e., the light source and viewer directly above the observed surface. Since

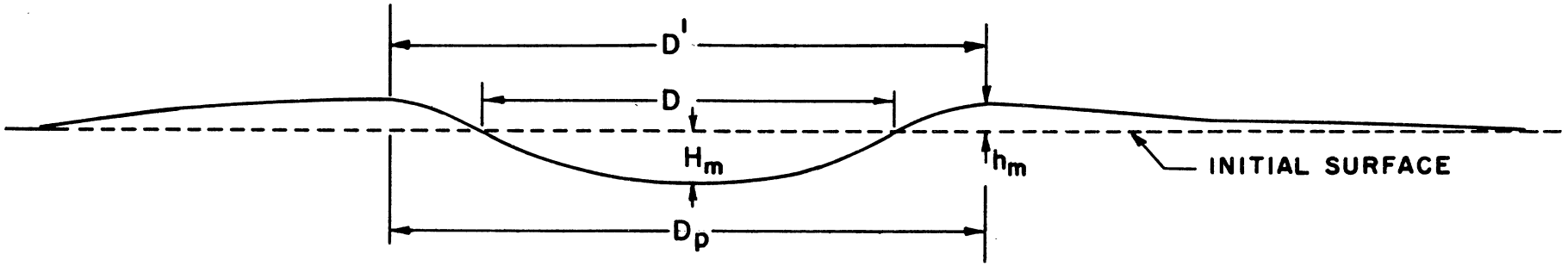

Figure 11. Actual artificial pit profile.

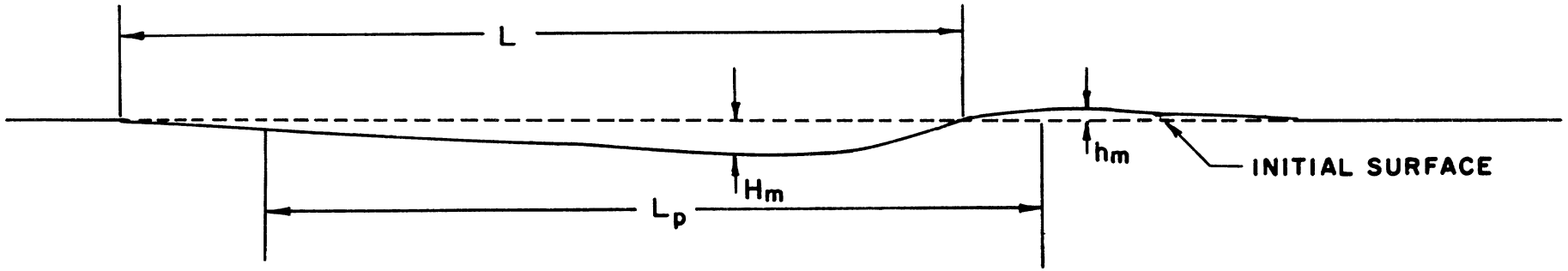

Figure 12. Actual cavitation pit profile. H_m and h_m are slightly exaggerated for clarity.

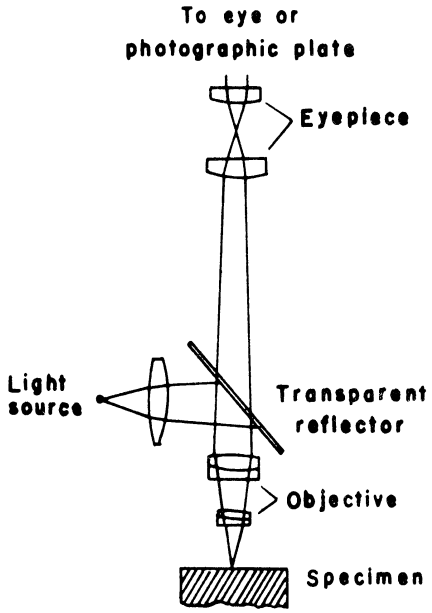

Figure 13. Optical features of a metallurgical microscope and metallograph camera.

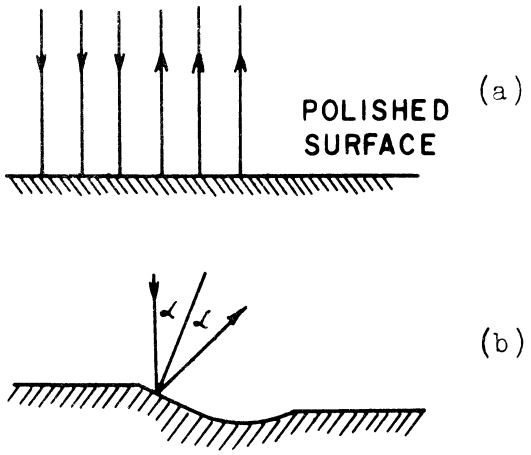

Figure 14. Schematic of regular and sidewise light reflection. (a) Light striking polished surface is reflected back to observer's eye or to photographic plate. (b) Light that strikes a sloping surface(as a pit crater) is reflected sidewise and does not return to the observer. Thus a pit crater appears dark.

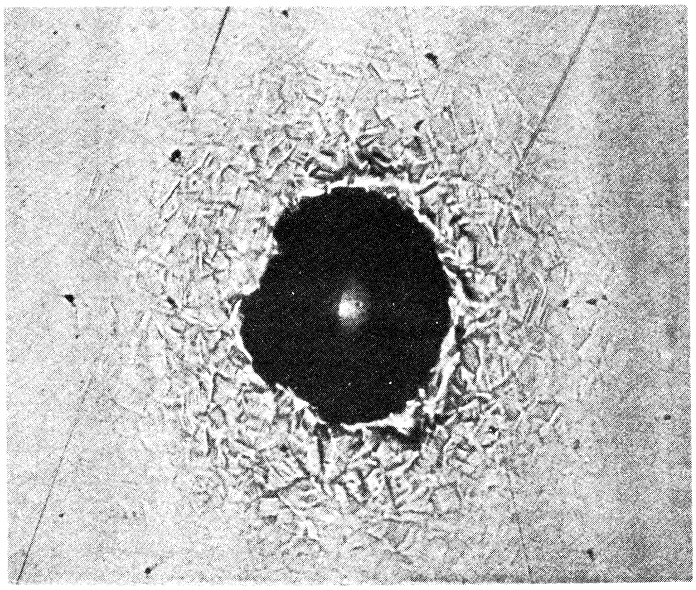

Figure 15. Macrograph of a "black spot" artificial pit 120X.

the tested samples are highly polished to a surface finish of about 2 microinches (rms), specular, or regular, reflections can be assumed for the light striking the observed surface. As can be seen from Figure 14, when the slope of the observed surface deviates enough from a horizontal position, the light will not be reflected back to the viewer.

As seen visually thru a microscope or from a photograph, a pit appears as a "black spot" (see Figure 15) on the observed surface with a white spot near its center (due to the horizontal portion of surface at the deepest point of the pit). The visually determined dimensions of a pit are measured to the edge of this "black" region.

For the artificial pit, as shown in Figure 11, light will not be reflected back to the viewer until the slope of the inner pit contour becomes essentially horizontal, i.e., near the ridge peaks of the pit. Thus the visual diameter of an artificial pit is greater than the actual crater diameter of the pit (as measured along the initial reference surface) and is approximately the distance from ridge peak to ridge peak of the artificial pit, or 1.22 times the actual pit diameter for the pit geometry shown in Figure 11, i.e., $D_p = 1.22D$. This theory is strengthened by the fact that for the pits examined it was found from the profi-corder traces that $D_p = 1.02D'$ or $D_p \doteq D'$, where D' is the distance between the ridge peaks of the artificial pits.

Cavitation pits are relatively much more shallow than the artificial pits observed, and also have propor-

tionately much smaller ridges (see Table IV), which exist, if at all, only partially around the pit crater. The shape of these cavitation pits explains the observed fact that their visual size is less than their actual size. Light is reflected back to the viewer as soon as the slope of the pit crater becomes small enough (see Figure 14). This occurs (see Figure 12) before the initial reference surface is reached, since generally, no ridge exists on at least one side of the pit crater, and where one does exist, it is proportionately much smaller than for the artificial pits, and thus because of its smaller slope, reflects light back to the viewer sooner, i.e., at a smaller diameter, than would an artificial pit ridge. Thus the visual size of a cavitation pit is slightly smaller than its actual size, while that of a hardness-indenter pit is slightly larger.

4.2 Crater and Ridge Volume

The volume loss proportionality constant was found to be $K = 7.346 \times 10^{-3}$. As shown in Table A-IV of the Appendix, the range of cavitation pits examined was from D_P = 1.1 to 10.3 mils. For these pits, the ratio of the ridge volume to the crater volume, v_R/v_C, ranged from 0.069 to 0.685, with an average of 0.328. Since McHugh[11] showed that the ratio of ridge volume to crater volume for an artificial pit (no metal removal) was approximately 1.0, it can be concluded that for all the pits examined (which included pits from the entire range of pit sizes thus far observed in

the mercury and water tests), metal was actually removed from each pit, and on the average about two thirds of the crater volume was actually removed.

4.3 Material Displacement

McHugh[11] also observed, in his artificial pit investigations, that vertical displacement of material (pit ridges) occurred up to 18 pit radii from the center of the pit. Ring and Biss[15] found that lateral displacement of material in the ridge of an artificial pit could be detected to only 3 to 4 pit radii from the center of the pit. This implies that the mechanism involved in the formation of an artificial pit causes the "upward" flow of metal to be greater than the "outward" flow.

In contrast, for the cavitation pits observed, the author detected vertical displacements of material only in the range of 3 to 5 pit radii from the center of the pits (see Figures 16 and 17 for typical proficorder traces of artificial and cavitation pits). This may indicate that the rapid stress rate present at the formation of cavitation pits does not allow sufficient time for the metal to flow and be displaced from the pit crater, thus leading to the "tearing" or "splashing" of metal from the surface of a cavitation sample. Other investigators[4,9,12,14,16] have also found that material displacement is much less for their dynamic tests than for the static loading present in the formation of the artificial pits considered by McHugh[11].

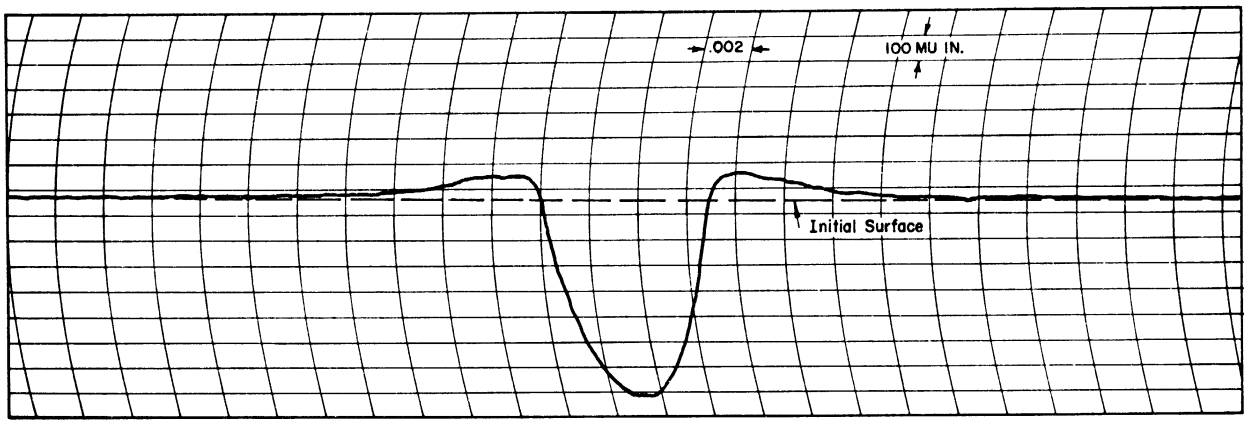

Figure 16. Typical proficorder trace of an artificial pit. Vertical scale: 100 microinches/division. Horizontal scale: 0.002"/division. ½X. Notice how far the ridges extend away from the pit crater, and the approximate symmetry of the ridges about the crater. Taken from McHugh(11).

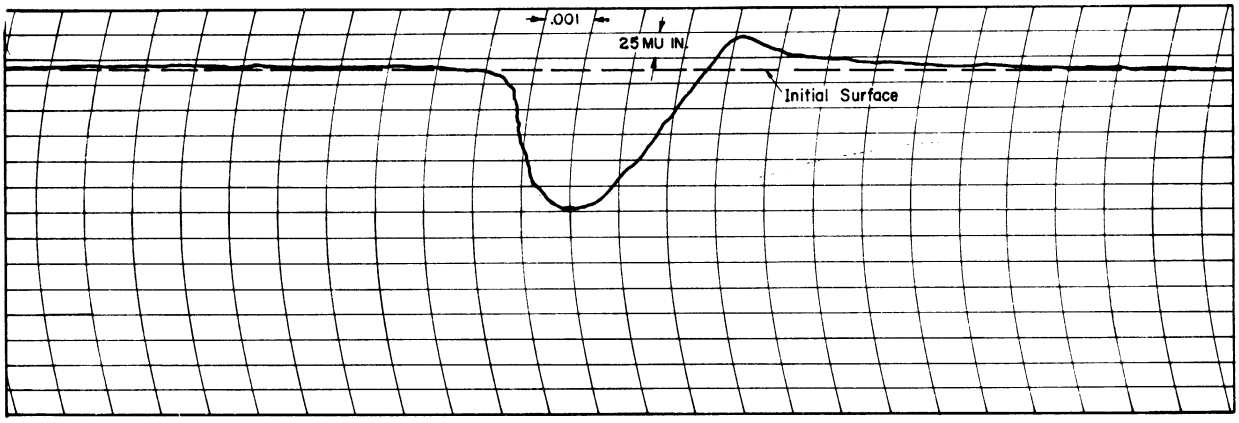

Figure 17. Typical proficorder trace of a cavitation pit. Vertical scale: 25 microinches/division. Horizontal scale: 0.001"/division. ½X. Note the smaller and non-symmetrical ridges (largest ridge is on downstream side of pit) of this cavitation pit as compared to the artificial pit illustrated in Figure 16.

The exact mechanism involved in the formation of cavitation pits and the removal of material there from is not presently known, but the following are possible theories which have been considered in the literature:

(1) Metal removal from a single bubble collapse because of:
   i) high shear stress due to high fluid velocity parallel to metal surface from an impinging fluid jet[3] due to a bubble collapsing on the metal surface[13].
   ii) high displacement velocity of metal around impact area, resulting in metal "splash"[2], due to a bubble collapse causing an impinging fluid jet[13] or shock wave[5,10] loading of the metal surface.

(2) Repeated shock wave[5,10] or impinging fluid jet[13] loading of metal surface, due to collapse of numerous bubbles, resulting in slab pitting from:
   i) inclusions or other surface imperfections[6,7].
   ii) surface fatigue failures[6,7,8].

4.4 Damage Rates

In section 3.4, the constant K_S, used to account for damage on the sides of test samples, was shown to be 3.601, i.e., there are on the average about 2.6 times as many pits on the sides of a test sample as on the polished surface. Since the area of the sides of a standard test sample is 8.04 times that of the polished surface, the "pitting rate" on the sides (per unit area) is only about 1/3, i.e., 2.601 / 8.04 = 0.324, of the "pitting rate" on the polished surface.

Two standard samples (surface roughness of sides about 20 microinches) were tested in mercury for 50 hours with

a total measured weight loss of 4.27 mg. Two specially prepared samples were polished on their sides as well as on their usually polished surface (surface roughness about 2 microinches) and were also tested for 50 hours under the same flow conditions as the standard samples mentioned above. They exhibited a total measured weight loss of 5.46 mg. This implies that the rougher finish of the sides of standard test samples would reduce the "pitting rate" on the sides to about 3/4, i.e., 4.27 / 5.46 = 0.782, of that on the polished surface if the sides and polished surface were exposed to the same flow conditions. This alone does not explain the 2/3 reduction in "pitting rate" on the sides reported above for standard specimens. Thus it appears that there are other factors involved, probably due to the different flow conditions to which the sides are exposed.

4.5 Pit Size Distribution in Mercury

To determine the RMS and RMC constants, the entire polished surface, of eight samples tested in mercury, was observed. The total number of pits on all the samples is tabulated in Table A-V of the Appendix. It is noted that there were about 10 times as many pits in the smallest size category (1) as in all the other categories combined. This may indicate that the pits in category 1 are those due to the collapse of very large (or at least energetic) individual bubbles, whereas the larger pits (especially those few in category 4) are due to a fatigue-type failure from the

collapse of very many smaller (or less energetic) bubbles near one location on the surface of a test sample.

4.6 Comparison of Pitting in Water and Mercury

Several interesting observations can be made from Table A-VIII of the Appendix. First note that there were more than twice as many pits in the smallest category 1, on the mercury samples than on the water samples, even though the water samples were tested 15 times as long (at the same flow and cavitation condition). This too may indicate that the pits in category 1 for samples tested in mercury are due to the collapse of very large, or energetic, individual bubbles (since the pits generally appear as circular craters), whereas in water, even the very large bubbles do not often produce enough energy (as do the mercury bubbles) to remove even small pieces of metal in a single blow. Thus it is implied that most of the damage to samples tested in water and in categories 2,3 and 4 for samples tested in mercury, is due to fatigue failures (because of their generally irregular contours) from the repeated blows of many collapsing bubbles, thus producing the larger pits observed in both water and mercury tests.

Consider Table V, which is a condensed form of Table A-VIII, for further clarification of the above. Here a linear extrapolation of the ratio of "pits on mercury samples to pits on water samples" has been made for equal test durations.

TABLE V

COMPARISON OF PITTING IN WATER AND MERCURY

Pit Size Category	Duration Hg	Duration H_2O	Total Hg	Pits H_2O	Hg/H_2O	$(Hg/H_2O)^*$
1	10	150	5100	2340	2.18	32.7
2	100	150	757	433	1.75	2.6
3	100	150	216	135	1.60	2.4
4	100	150	164	103	1.59	2.4

Note that for pit size categories 2,3 and 4 (most of the pits in these categories in both mercury and water are hypothesized to be due to fatigue failures), the extrapolated ratio of "pits on mercury samples to pits on water samples" remains essentially constant, but the pitting rate for mercury is about $2\frac{1}{2}$ times greater than for water. However, for pit size category 1, the ratio is much larger and is about 32.7. Thus many more pits in category 1 are formed in mercury than in water, which may indicate that these pits are mostly due to a single bubble collapse in mercury and many bubble collapses (fatigue failures) in water.

It is also noted from Table A-VIII, that the sides to polished surface average pitting ratio, for water and mercury combined, varied only between 2.45 and 2.79 for all four pit size categories, even though opposite trends exist in water and mercury since the ratio of pits on sides to pits on

*Linear extrapolation to equal test durations of 150 hours.

polished surface (1) tends to decrease as pit size increases for mercury tested samples, and (2) tends to increase as pit size increases for water tested samples. This is probably due to the different flow conditions to which the sides are exposed to in the two fluids (water and mercury).

5.0 WORKING RELATIONS FROM DERIVED EQUATIONS

In this section, the equations derived in section 2 will be expanded into working relations by substitution of the empirical constants (Table VI) determined in section 3. In the present damage tests, samples of austenitic stainless and mild carbon steel, plexiglas, and of a columbium-1% zirconium alloy were tested. Thus where sample density enters into one of the derived equations, suitable equations will be formed for each separate material.

TABLE VI

SUMMARY OF EMPIRICAL CONSTANTS

$C_1 = 0.5216$ mils^3	$S_1 = 0.6480$ mils^2	$K_P = 1.172$	
$C_2 = 6.0363$ mils^3	$S_2 = 3.1525$ mils^2	$K_S = 3.601$	
$C_3 = 71.1547$ mils^3	$S_3 = 16.4799$ mils^2	$K = 7.346 \times 10^{-3}$	
$C_4 = 334.4513$ mils^3	$S_4 = 46.6233$ mils^2		

5.1 Weight Loss

In section 2.1, the weight loss due to the pits on only the polished surface of a damage specimen was shown to be:

$$WL' = \rho K K_P^3 (n_1 C_1 + n_2 C_2 + n_3 C_3 + n_4 C_4) \qquad (2.1\text{-}7)$$

WL' thus becomes:

$$WL' = \rho(7.346 \times 10^{-3})(1.172)^3(.5216n_1 + 6.0363n_2 + 71.1547n_3 + 334.4513n_4)$$

or $$WL' = \rho(11.8256 \times 10^{-3})(.5216n_1 + 6.0363n_2 + 71.1547n_3 + 334.4513n_4) \text{ mils}^3$$

The densities of the materials tested are given in Table VII.

TABLE VII

DENSITY OF TEST SPECIMEN MATERIALS

Material	grams/cc	grams/mil^3
Stainless steel(Type 302)	7.85	1.285×10^{-7}
1010 Carbon steel	7.85	1.285×10^{-7}
Plexiglas	1.23	0.202×10^{-7}
Columbium-1% Zirconium	8.72	1.429×10^{-7}

Thus the respective weight losses due to pitting of only the polished surface becomes:

$$WL'_{SS,CS} = (1.285 \times 10^{-7})(11.8256 \times 10^{-3})(.5216n_1 + 6.0363n_2 + 71.1547n_3 + 334.4513n_4) \text{ grams}$$

or $$WL'_{SS,CS} = 15.1959 \times 10^{-10}(.5216n_1 + 6.0363n_2 + 71.1547n_3 + 334.4513n_4) \text{ grams} \qquad (5.1\text{-}1a)$$

Similarly:

$$WL'_{Plex} = 2.3888 \times 10^{-10}(.5216n_1 + 6.0363n_2 + 71.1547n_3 + 334.4513n_4) \text{ grams} \qquad (5.1\text{-}1b)$$

and $$WL'_{Cb\text{-}1Zr} = 16.8988 \times 10^{-10}(.5216n_1 + 6.0363n_2 + 71.1547n_3 + 334.4513n_4) \text{ grams} \qquad (5.1\text{-}1c)$$

The total weight loss equations for each material can be obtained from equation (2.1-8), which is merely the factor K_S (to account for damage to the sides of a test sample) times the weight loss due to pitting to only the polished surface of a damage specimen, or:

$$WL_{SS,CS} = K_S WL'_{SS,CS}$$

Thus:

$$WL_{SS,CS} = (3.601)(15.1959 \times 10^{-10})(.5216n_1 + + 6.0363n_2 + 71.1547n_3 + 334.4513n_4)$$

or $$WL_{SS,CS} = 54.7204 \times 10^{-10}(.5216n_1 + 6.0363n_2 + +71.1547n_3 + 334.4513n_4) \text{ grams} \qquad (5.1\text{-}2a)$$

Similarly:

$$WL_{Plex} = 8.6021 \times 10^{-10}(.5216n_1 + 6.0363n_2 + +71.1547n_3 + 334.4513n_4) \text{ grams} \qquad (5.1\text{-}2b)$$

and $$WL_{Cb\text{-}1Zr} = 60.8526 \times 10^{-10}(.5216n_1 + 6.0363n_2 + +71.1547n_3 + 334.4513n_4) \text{ grams} \qquad (5.1\text{-}2c)$$

5.2 Mean Depth of Penetration

In section 2.2, the mean depth of penetration, due to pitting of only the polished surface of a test sample, was shown to be:

$$MDP' = KK_P^3(n_1C_1 + n_2C_2 + n_3C_3 + n_4C_4) / A_{PS} \qquad (2.2\text{-}1)$$

where: $A^*_{PS} = 0.0372 \text{ in}^2 = 3.72 \times 10^4 \text{ mils}^2$, and the other

*From L.L. Barinka memo to U-M Project 03424 File, November 1961.

constants are as previously listed in Table VI.

MDP' thus becomes:

$$MDP' = (7.346 \times 10^{-3})(1.172)^3(.5216n_1 + 6.0363n_2 + 71.1547n_3 + 334.4513n_4) / 3.72 \times 10^4$$

or $$MDP' = 3.1789 \times 10^{-7}(.5216n_1 + 6.0363n_2 + 71.1547n_3 + 334.4513n_4) \text{ mils} \qquad (5.2\text{-}1)$$

From equation (2.2-2), the mean depth of penetration for an entire test sample can be obtained as follows:

$$MDP = KK_P^3K_S(n_1C_1 + n_2C_2 + n_3C_3 + n_4C_4) / A_T \qquad (2.2\text{-}2)$$

where: $A_T = 0.3362 \text{ in.}^2 = 3.362 \times 10^5 \text{ mils}^2$, and the other constants are as previously listed in Table VI.

$$MDP = (1.1826 \times 10^{-2})(3.601)(.5216n_1 + 6.0363n_2 + 71.1547n_3 + 334.4513n_4) / 3.362 \times 10^5$$

or $$MDP = 1.2666 \times 10^{-7}(.5216n_1 + 6.0363n_2 + 71.1547n_3 + 334.4513n_4) \text{ mils} \qquad (5.2\text{-}2)$$

5.3 Percent Damaged Area

In section 2.3, the percent damaged area due to the pits on only the polished surface of a test sample was shown to be:

$$PDA' = 25\pi K_P^2(n_1S_1 + n_2S_2 + n_3S_3 + n_4S_4) / A_{PS} \ \% \qquad (2.3\text{-}1)$$

All constants have previously been listed in this section, thus PDA' becomes:

$$PDA' = 25\pi(1.172)^2(.6480n_1 + 3.1525n_2 + + 16.4799n_3 + 46.6233n_4) / 3.72 \times 10^4$$

or $$PDA' = 29.0006 \times 10^{-4}(.6480n_1 + 3.1525n_2 + + 16.4799n_3 + 46.6233n_4) \quad \% \qquad (5.3\text{-}1)$$

The total percent damaged area of a test specimen is given by equation (2.3-2):

$$PDA = 25\pi K_P^2 K_S(n_1S_1 + n_2S_2 + n_3S_3 + n_4S_4) / A_T \quad \% \qquad (2.3\text{-}2)$$

All constants have previously been listed in this section, thus PDA becomes:

$$PDA = 25\pi(1.172)^2(3.601)(.6480n_1 + 3.1525n_2 + + 16.4799n_3 + 46.6233n_4) / 3.362 \times 10^5$$

or $$PDA = 11.5551 \times 10^{-4}(.6480n_1 + 3.1525n_2 + + 16.4799n_3 + 46.6233n_4) \quad \% \qquad (5.3\text{-}2)$$

6.0 SAMPLE CALCULATIONS USING THE DERIVED EQUATIONS

In this section some numerical substitutions will be made into the previously derived equations to determine whether any restrictions should be placed on their use. The following three equations will be considered.

$$WL_{SS} = 54.7204 \times 10^{-10}(.5216n_1 + 6.0363n_2 + \\ + 71.1547n_3 + 334.4513n_4) \text{ grams} \qquad (5.1\text{-}2a)$$

$$MDP = 1.2666 \times 10^{-7}(.5216n_1 + 6.0363n_2 + \\ + 71.1547n_3 + 334.4513n_4) \text{ mils} \qquad (5.2\text{-}2)$$

$$PDA = 11.5551 \times 10^{-4}(.6480n_1 + 3.1525n_2 + \\ + 16.4799n_3 + 46.6233n_4) \ \% \qquad (5.3\text{-}2)$$

6.1 Calculation of Maximum Values of WL, MDP, and PDA

The maximum weight loss of a damaged sample will be approximated by considering each pit size categoty individually.

The total sample weight loss due to one pit on the polished surface in the smallest pit size category is given by the first term of equation (5.1-2a).

$$wl_1 = 54.7204 \times 10^{-10} \left[.5216(1)\right]$$
$$wl_1 = 28.5425 \times 10^{-10} \text{ grams}$$

The percent damaged area due to $n_1 = 1$ is:

$$pda_1 = 11.5551 \times 10^{-4} \left[.6480(1)\right]$$

$$pda_1 = 7.4877 \times 10^{-4} \ \%$$

After observing many heavily damaged specimens, particularly in the mercury tests, it is estimated that the maximum percent damaged area due to pits in pit size category 1 is about 90%. Thus the maximum contribution of the smallest pit size category to the total sample weight loss is (assuming that only a single layer of pits is present):

where: $n_1 = 90\% \ / \ 7.4877 \times 10^{-4}\% = 120{,}197$ pits

$$WL_1 = 28.5425 \times 10^{-10}(120{,}197)$$

$$WL_1 = 34.3073 \times 10^{-5} \text{ grams}$$

$$WL_1 = 0.3431 \text{ mg.}$$

Note that since the RMC constant for pits with $0.1 < D_p < 0.46$ mils would be about 1/25 the RMC constant for category 1, and since the number of pits of this size is usually less than 300, their contribution to the weight loss is negligible.

A consideration of all the available pit count tabulations of damaged specimens indicates that the maximum number of pits in pit size categories 2,3, and 4 are:

$$n_2 = 200 \ , \quad n_3 = 30 \ , \quad n_4 = 10$$

Thus the contribution to the total weight loss of

each of these pit size categories is:

$$WL_2 = 54.7204 \times 10^{-10} \left[6.0363(200)\right]$$
$$WL_2 = 0.6606 \times 10^{-5} \text{ grams}$$
$$WL_2 = 0.0066 \text{ mg.}$$

$$WL_3 = 54.7204 \times 10^{-10} \left[71.1547(30)\right]$$
$$WL_3 = 1.1681 \times 10^{-5} \text{ grams}$$
$$WL_3 = 0.0117 \text{ mg.}$$

$$WL_4 = 54.7204 \times 10^{-10} \left[334.4513(10)\right]$$
$$WL_4 = 1.8301 \times 10^{-5} \text{ grams}$$
$$WL_4 = 0.0183 \text{ mg.}$$

Summing the contributions of the four pit size categories gives an approximation of the maximum total weight loss of a damaged sample, which can be calculated from the derived equations within their limit of applicability.

$$WL_{SS_{max}} = WL_1 + WL_2 + WL_3 + WL_4$$
$$WL_{SS_{max}} = 0.3431 + 0.0066 + 0.0117 + 0.0183$$
$$WL_{SS_{max}} = 0.3797 \text{ mg.}$$

The maximum mean depth of penetration corresponding to this maximum weight loss of 0.3797 mg. is given by equation (5.2-2), where the n_i's are as above:

$$MDP_{max} = 1.2666 \times 10^{-7} \left[.5216(120,197) + 6.0363(200) + 71.1547(30) + 334.4513(10)\right] \text{ mils}$$

$$MDP_{max} = 1.2666 \times 10^{-7}(6.2695 + 0.1207 + + 0.2135 + .3345) \times 10^{4}$$

$$MDP_{max} = 1.2666 \times 10^{-3}(6.9382) \text{ mils}$$

$$MDP_{max} = 8.7879 \times 10^{-3} \text{ mils}$$

or $$MDP_{max} = 8.7879 \text{ microinches}$$

The maximum percent damaged area of a test specimen for the n_i's assumed above is given by equation (5.3-2).

$$PDA_{max} = 11.5551 \times 10^{-4} \left[.6480(120,197) + 3.1525(200) + +16.4799(30) + 46.6233(10)\right] \quad \%$$

$$PDA_{max} = 11.5551 \times 10^{-4}(7.7888 + 0.0631 + 0.0494 + +0.0466) \times 10^{4} \quad \%$$

$$PDA_{max} = 11.5551 \times 7.9479 \quad \%$$

$$PDA_{max} = 91.8388 \quad \%$$

6.2 Discussion of Calculations

From the above rough numerical calculations, we found that:

$$WL_{SS_{max}} = 0.38 \text{ mg.}$$
$$MDP_{max} = 8.8 \text{ microinches}$$
$$PDA_{max} = 91.8 \%$$

In section 6.1, PDA was assumed to be large to obtain maximum values for the above damage parameters. For actual damaged samples, the percent damaged area, as approx-

imated by observing the samples under high magnification, appears to range between 20 and almost 100%.

The maximum depth of pit craters, as measured from proficorder traces of the pit profiles, varies from about 20 microinches (pit size category 1) to about 300 microinches (pit size category 4). Thus the value of MDP_{max} = 8.8 microinches, appears reasonable considering that it is the volume of all the pits divided by the total exposed surface area.

To determine how well the weight loss equations fit the actual weight loss curves of damaged samples, consider Figure 18.

Curve A typifies a sample that receives significant damage throughout its test duration and which is countable for its entire test duration. Curve B is typical of a sample receiving more damage than sample A, becoming so damaged that pit counting cannot be continued after about 25 hours of testing. Some samples follow curves of type B to say point b, and then increase rapidly along a curve as B'.

The value of $WL_{SS_{max}}$ = 0.38 mg. obtained from our derived equation corresponds in proper order of magnitude to curve A, but not to curves B or B'. Thus it appears that the equation can be used to describe the weight loss (for other than quite short tests) for only those samples typified by weight loss curves similar to curve A.

As mentioned above, samples which follow curve type B become uncountable after about 25 hours of testing, whereas samples which follow curve type A retain a well-defined sur-

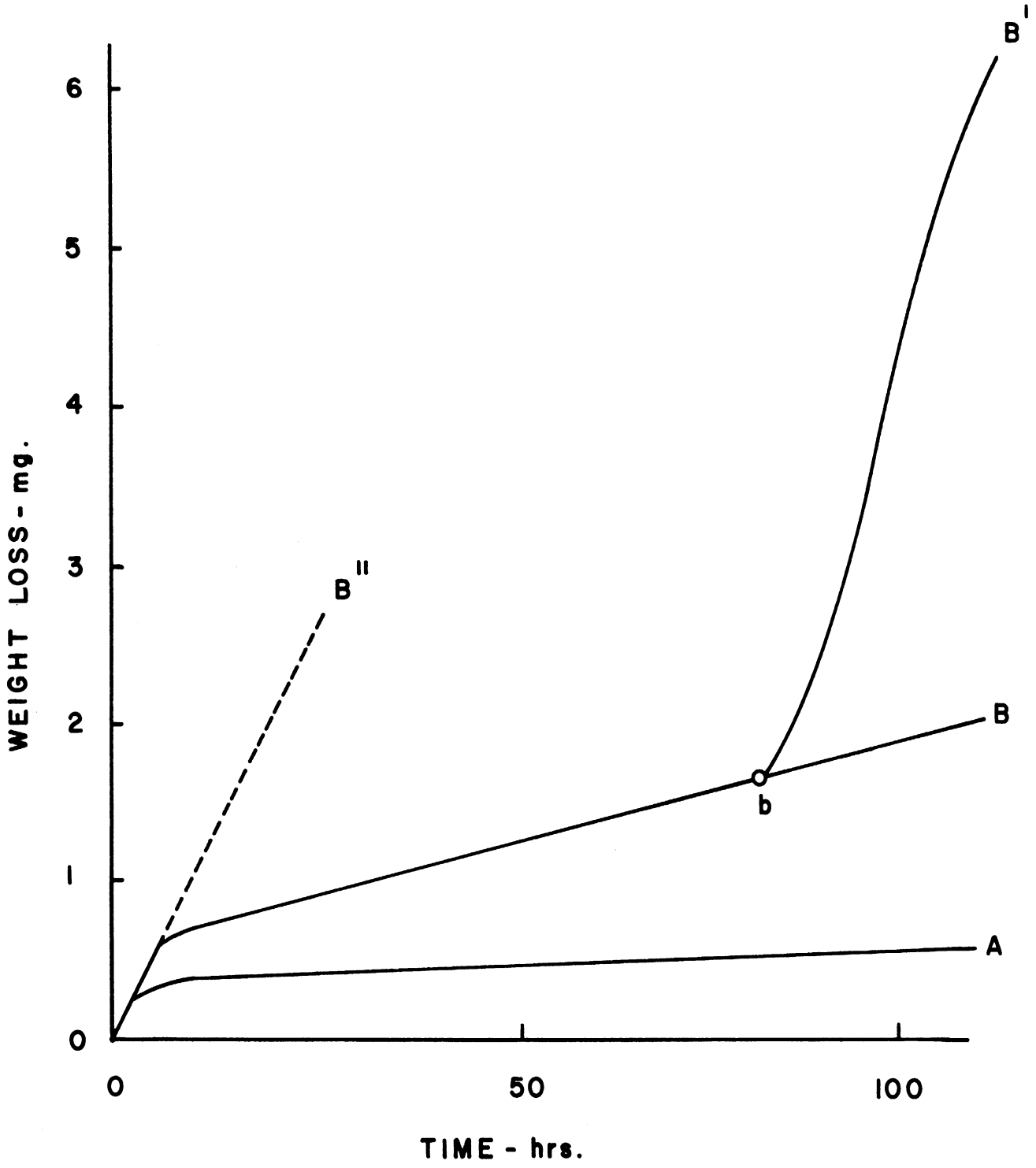

Figure 18. Schematic drawing of typical actual weight-loss curves for samples tested in mercury.

face and edge finish, and can be pit counted throughout their test duration, i.e., for several hundred hours. In general, curve type A is typical of samples tested in mercury at "visible initiation" and "cavitation to nose" test conditions, and curves of type B and B' are typical of samples tested in mercury at "standard" and "cavitation to back end" test conditions (see section 1.0 and Figure 2 for definitions of each cavitation condition).

The author also examined proficorder traces, made by Cramer[1] and Walsh[18], of pit profiles of samples tested in water, and found that the pit contours are similar to the profile of the pits on mercury tested samples. Since all samples tested in water accumulate much less damage than those tested in mercury, and retain a well defined surface and edge finish, it appears that the derived equations can be used for all test conditions in water.

In summary, the application of the derived equations is restricted to the following cases:

(1) Samples tested in water at any cavitation condition and for any velocity and test duration yet attained.

(2) Samples tested in mercury at only "visible initiation" and "cavitation to nose" cavitation conditions for long test duration.

(3) Samples tested in mercury at "standard" and "cavitation to back end" test conditions for short initial test durations of approximately

5 hours, i.e., until the surface and edges cannot be well-defined, and it can no longer be assumed that the pits do not significantly overlap.

Thus the equations cannot be used, in the context of the present tests, only in the case of samples tested in mercury for long durations at "standard" and "cavitation to back end" test conditions.

Thus it is expected that the visible pitting damage to a damage specimen is proportional to the actual weight loss of the damaged sample as long as the sample is not so severely damaged that its surface and edges cannot be well-defined.

It is also believed that for the heavily damaged samples, curve types B and B', the pitting is also directly proportional to the weight loss, but that the calculated value of maximum weight loss will not agree with the actual weight loss only because accurate pit count tabulations cannot be obtained for the more heavily damaged samples*. Three factors which lead to inaccurate pit count tabulations on heavily damaged samples are:

i) No account of the possible over-lapping of pits of similar size(i.e., layers of pits) can be made. Figures 19 and 20 are photomicrographs of large shallow pits which show the formation of small

---

*When the body of damage data available is reduced, using the equations derived in this report, and compared to the measured weight losses, it is expected that more definitive statements can be made in these different regards.

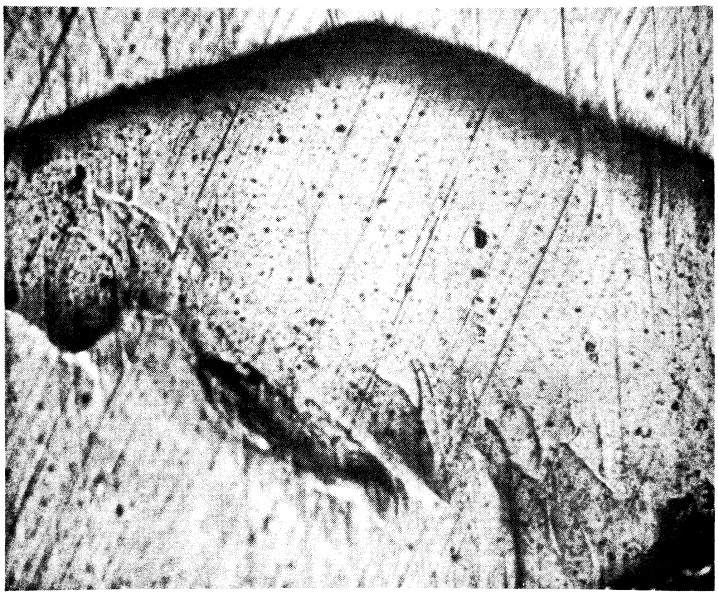

Figure 19. Macrograph showing small pits on the bottom of a large shallow crater. Stainless steel specimen #63. Cavitation to nose. Throat velocity-34 fps. 100 hours test duration in mercury. 300X.

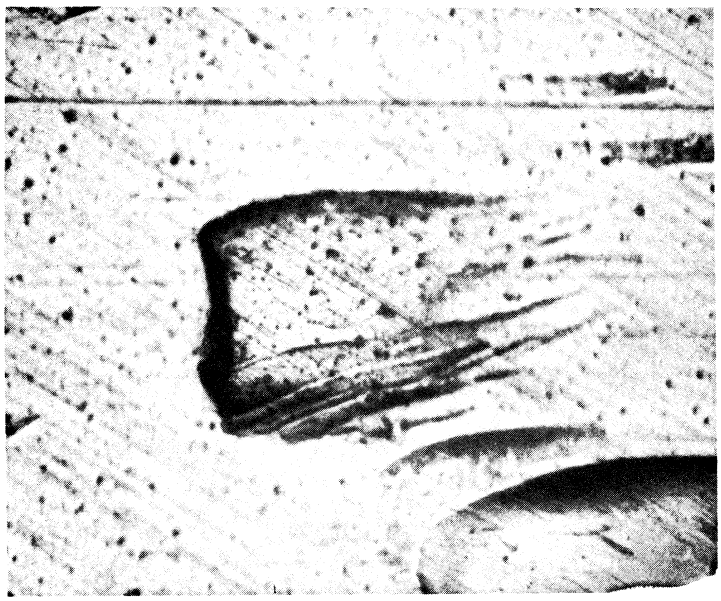

Figure 20. Macrograph showing small pits on the bottom of a large shallow crater. Same sample as shown in Figure 19.

pitting on the bottom of the large pit craters. Figure 21 shows two over-lapping pits of similar size.

ii) For heavily damaged samples, a dark band occurs along the edge of the sample due to a "rounding" of the edges. Not only is the pitting in this region undeterminable, but also the amount of material removed in the "rounding" of the edges cannot be determined by the visual methods thus far developed. Figure 9 shows this dark band along the sample edge, and Figure 22 is a microsection through a sample that shows the actual rounding of the edge.

iii) A brown smudging of the polished surface, which tends to obscure pits making accurate tabulations difficult, has also been observed on some specimens in regions of light cavitation. The smudging later develops into colored bands, similar in appearance to oxide formation on steel from heating. Figure 23b is a photomicrograph of the same location as Figure 23a, but was taken after 9 additional hours of wear, and indicates how the smudging covered and obscured the pits that were visible in Figure 23a. (A more detailed description of the discoloring process is given in Reference 8).

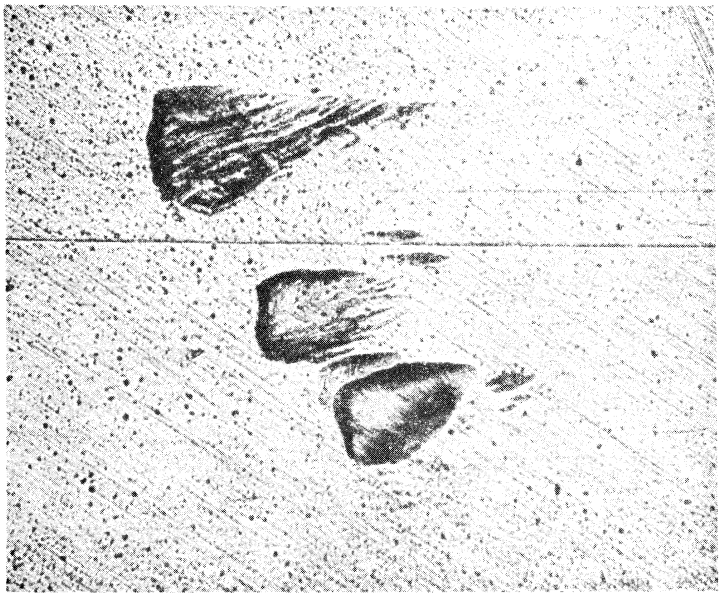

Figure 21. Macrograph showing the over-lapping of two similar sized pits. Same sample as shown in Figure 19, except at 120X. Notice how the large pit at the bottom of the picture formed on top of part of a pit about half its size.

Figure 22. Microsection illustrating the "rounding" of a samples edge. Stainless steel specimen #26. Standard cavitation. Throat velocity 97.2 fps. 12 hours test duration in water. Etched. 1000X.

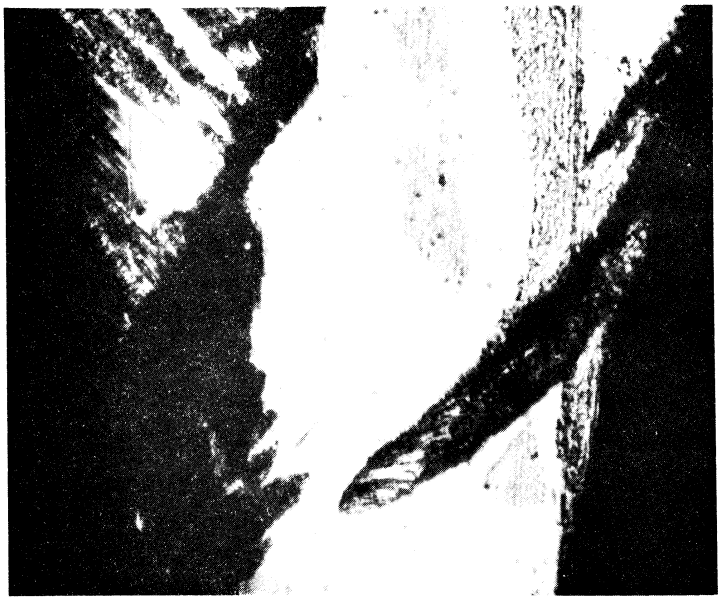

(a)

(b)

Figure 23. Macrographs illustrating the "smudging" of the polished surface of a test specimen. Columbium-1%Zirconium specimen #14. Standard cavitation. Throat velocity-48 fps. 120 X. (a) after 1 hour of testing in mercury. (b) after 10 hours of testing in mercury. Notice how dark smudging in b covers and obscures some of the pits visible in a.

6.3 Discussion of Actual Weight Loss Curves

At this point some consideration will be given to the typical weight loss curves illustrated in Figure 18. The difference in "wear rate" indicated by curves A and B (considering sample material and flow rate to be constant for all curves) is explained simply by the different cavitation conditions used.

Some samples have been observed which exhibit a relatively uniform wear rate illustrated by curve B to say point b, and then exhibit a large increase in wear rate after point b. It is believed that this is due to a "gross" fatigue type failure of the surface encompassing areas much larger than single pits, from the collapse of many cavitation bubbles in localized areas.

The surface failure is ascribed to fatigue because the sharp increase in weight loss occurs only after many hours of testing and is characterized by the removal of relatively large amounts of material from the sample which are much greater than the previously observed pits. Figures 24 and 25 illustrate this type of "gross" failure. Incidentally this type of failure may be that observed by various previous investigators in reporting a cavitation damage incubation period. Such an apparent period would result from extrapolating the sharply rising portion of the curve back to zero weight loss. If direct weight loss measurements only were used, the losses prior to "b" might not be detected.

Note that both curves A and B exhibit a large

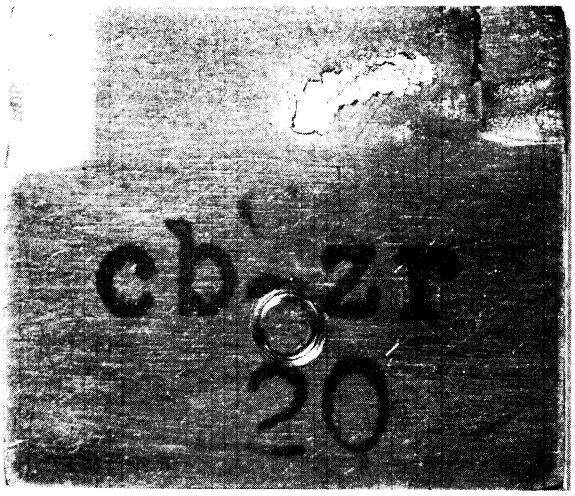

Figure 24. Macrograph of a "gross" type fatigue failure. Columbium-1%Zirconium specimen #20. Cavitation to nose. Throat velocity-48 fps. 50 hours test duration in mercury. 4X. Flow is from left to right.

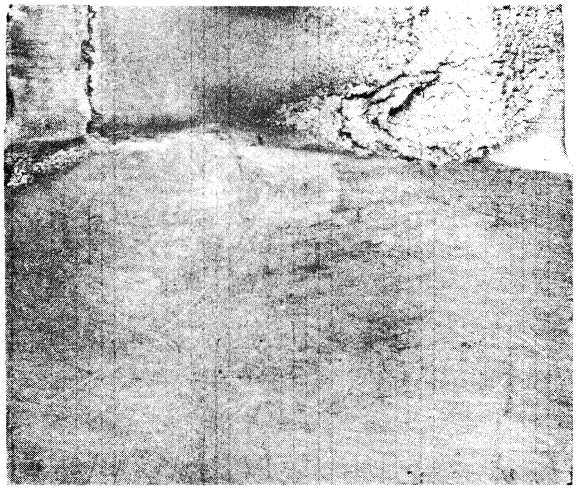

Figure 25. Macrograph of a "gross" type fatigue failure. Columbium-1%Zirconium specimen #1. Standard cavitation. Throat velocity-34 fps. 100 hours test duration in mercury. 4X. Flow is from left to right.

"wear rate" over their first few hours of testing and then exhibit a smaller, steady "wear rate" over the remainder of their test duration (unless the above gross fatigue failure occurs). The following two explanations are proposed for the small, but rapid, initial weight loss.

1. Inclusions, (or other imperfections) that are at or near the surface of a sample, can be removed from the material initially rather easily due to the collapse of relatively few bubbles near the inclusion, and show up as a large initial weight loss, followed by the "normal" wear rate of the sample material throughout the remainder of the test duration.
2. There may be some effect due to work-hardening of the surface. Thus in the extreme it might be that curve B" is the "normal" wear rate of the sample material, and that the sample is locally surface-hardened to some extent by the cavitation and thus exhibits a lower wear rate (curve B" to B) during the remainder of the test. Such surface hardening would help to explain the later brittle-fatigue-type of failure that occurs on some samples (curve B to B').

More investigation is certainly needed to establish the possible validity of either of the above mechanisms.

7.0 CONCLUSIONS

The following conclusions can be drawn from the present investigation:

(1) For artificial pits, the visual pit diameter (D_p) is actually closely equal to the distance between the ridge peaks (D') of the pits.

(2) Metal was actually removed from all of the cavitation pits traced with the linear proficorder.

(3) According to the available evidence, material is vertically displaced from the crater of a cavitation pit to only about $\frac{1}{4}$ the radial distance that applies to an artificial pit crater.

(4) The pitting rate per unit area on the sides of a damage specimen is only about 1/3 that on the polished surface.

(5) The contour of pits produced by either water or mercury cavitation damage is closely similar.

(6) Cavitation pitting, according to present evidence*, is directly proportional to the weight loss of a test sample whose shape remains well-

---

*It is hoped that an equality can soon be verified by comparison between calculated and directly measured weight loss. A proportionality was exhibited in irradiated specimen tests[17].

defined throughout its test duration (no gross rounding of edges or over-lapping of pits in layers of damage).

(7) The derived equations are applicable to samples under the conditions defined in item (6) above.

(8) The majority of the weight loss of severly damaged samples is due to "layers" of pitting on the surfaces and to "rounding" of the samples edges.

The following are not as well supported as those above, but are given as possible theories:

(1) The small pits (pit size category 1) on samples tested in mercury are due to the collapse of one sufficiently large or energetic bubble.

(2) Most of the larger pits (categories 2,3, and 4) on samples tested in both water and mercury are due to localized fatigue-type failures.

(3) The abrupt change in weight loss typified by curve B' on Figure 18 is due to a large-scale, "gross" type of fatigue failure.

(4) The phenomenon of a small but rapid initial weight loss followed by a more gradual wear rate is due to either inclusions, or other imperfections, ejected from the surface of the material by the early phases of cavitation, or perhaps to a surface hardening effect of the

sample material as cavitation proceeds.

(5) Surface finish, at least in the range tested, does not seem an important parameter for sensitivity to damage. In fact in the present tests, the smoother the surface the more damaged received.

8.0 LIST OF REFERENCES

1. Cramer, V. F., and Hammitt, F. G., "Cavitation Pit Diameter - Depth Observations For Stainless Steel In Water", Internal Report #9, ORA Project 03424, University of Michigan, August 1961.

2. Engel, O. G., "Mechanism of Rain Erosion, Part 2, A Critical Review of Erosion by Water Drop Impact",WADC Technical Report 53-192, National Bureau of Standards, August 1953.

3. Engel, O. G., "Mechanism of High-Speed-Waterdrop Erosion of Methyl Methacrylate Plastic", Journal of Research of the National Bureau of Standards, Vol. 54, No. 1, January 1955, pp. 51-59.

4. Engel, O. G., "Erosion Damage to Solids Caused by High-Speed Collision With Rain", Journal of Research of the National Bureau of Standards, Vol. 61, No. 1, July 1958, pp. 47-52.

5. Gilmore, F. R., "The Growth or Collapse of a Spherical Bubble In a Viscous Compressible Liquid", Report No. 26-4, Hydrodynamics Laboratory, California Institute of Technology, April 1952.

6. Hammitt, F. G., et. al., "Cavitation Damage Tests With Water in a Cavitating Venturi", Technical Report #4, ORA Project 03424, University of Michigan, March 1962.

7. Hammitt, F. G., "Observations on Cavitation Damage in a Flowing System", ASME Paper No. 62-WA-100, 1962, (to be published ASME Jour. Basic Engr.).

8. Hammitt, F. G., et. al., "Cavitation Damage to Cb-1Zr Alloy in Mercury in a Venturi", Final Report, ORA Project 05122, University of Michigan, August 1962.

9. Jones, F. H. S., "Some Comments on Cratering", Suffield Special Publication 22, Defence Research Board of Canada, Suffield Experimental Station, Ralston Alberta, April 1962.

10. Knapp, R. T., "Recent Investigations of the Mechanics of Cavitation and Cavitation Damage", Trans. ASME, Vol. 77, 1955, pp. 1045-1054.

11. McHugh, R. J., "Analysis of Proficorder Traces of Hardness Indenter Pits", M.E. 600 Project Report, Mechanical Engineering Department, University of Michigan September 1962.

12. Merritt, M. L., Murphey, B. F., Vortman, L. J., "Cratering With Chemical Explosives", Report No. UCRL-5676, Lawrence Radiation Laboratory, University of California, 1960.

13. Naude, C. F., and Ellis, A. T., "On the Mechanism of Cavitation Damage by Non-hemispherical Cavities Collapsing in Contact With a Solid Boundry", Trans. ASME, Jour. Basic Engr., December 1961, pp. 648-656.

14. Perkins, B. , "A New Technique For Studying Crater Phenomena", Technical Note No. 880, Ballistic Research Laboratories, Aberdeen Proving Ground, Maryland, March 1954.

15. Ring, H. M., and Biss, V. A., "The Effect of the Hardness Indenter on the Surrounding Surface of Austenitic Stainless Steel", Memo Report, ORA Project 03424, University of Michigan, February 1963.

16. Tolansky, S. , "Surface Microtopography", International Science and Technology, September 1962, pp. 32-39.

17. Walsh, W. J., and Hammitt, F. G., "Cavitation and Erosion Damage Measurements With Radioisotopes", Trans. ANS, Vol. 4, No. 2, November 1961, p. 247.

18. Walsh, W. J., "Analysis of Profilometer Data For Cavitation Pits", Internal Report #2, ORA Project 03424, University of Michigan, September 1960.

9.0 APPENDIX

LIST OF TABLES

TABLE A-I

PROFILE DATA FOR ARTIFICIAL PITS ON 302-STAINLESS STEEL*

Pit	Trace	D	D'	D_P	D_P/D	D_P/D'
1-1	1-13	7.126	8.500	8.333	1.169	0.980
1-2	2-15	7.250	8.562	8.594	1.185	1.004
3-3	3-17	7.688	9.126	9.635	1.253	1.056
3-4	4-18	7.376	9.000	9.375	1.271	1.042
					4.878	4.082

Pit	Trace	D	H_m	h_m	D/H_m	D/h_m	H_m/h_m
1-1	1-13	7.126	0.875	0.125	8.144	57.008	7.000
1-2	2-15	7.250	0.906	0.109	8.002	66.513	8.311
3-3	3-17	7.688	1.031	0.171	7.456	44.959	6.029
3-4	4-18	7.376	1.031	0.125	7.154	59.008	8.248
					30.756	227.488	29.588

Average $D_P/D = 4.878 / 4 = 1.22$

Average $D_P/D' = 4.082 / 4 = 1.02 \doteq 1$

Average $D/H_m = 30.756 / 4 = 7.689$

Average $D/h_m = 227.488 / 4 = 56.872$

Average $H_m/h_m = 29.588 / 4 = 7.397$

TABLE A-II

PROFILE DATA FOR CAVITATION PITS ON 302-STAINLESS STEEL*

Pit	Trace	L	H_m	h_m	L_P	L_P/L	L/H_m	L/h_m	H_m/h_m
#2	1-10	2.25	.125	.050	1.9	.844	18.0	45	2.5
#4	1-26a	6.63	.347	.005	5.8	.874	19.1	1326	69.4
#5	1-36	4.25	.216	.025	3.4	.800	19.7	170	8.6
#11	2'-13	7.75	.181	.005	6.05	.780	42.8	1550	36.2
#12	2'-17	6.38	.191	.034	6.45	1.010	33.4	188	5.6
#13	2'-31	10.5	.228	.008	8.55	.814	46.1	1313	28.0
						5.122			

Average $L_P/L = 5.122 / 6 = 0.853$

$K_P = L/L_P = 1 / 0.853 = 1.172$

*All dimensions are in mils.

TABLE A-III

DATA FOR RIDGE & CRATER VOLUMES OF 14 CAVITATION PITS FROM PROFICORDER TRACES OF STAINLESS STEEL SAMPLE #63

Pit	Trace	Planimeter* a_R	Planimeter* a_C	Area x10^9 in.^{2} a_R	Area x10^9 in.^{2} a_C	Mean Areas a_R	Mean Areas a_C	Vol. x10^{12} in.^{3} V_R	Vol. x10^{12} in.^{3} V_C
#1	1-4	0	0	0	0				
						15.0	0	15.0	0
	1-5	7.5	0	30.0	0				
						20.6	2.8	20.6	2.8
	1-6	2.8	1.4	11.2	5.6				
						28.6	108.8	28.6	108.8
	1-7	11.5	53.0	46.0	212.0				
						39.4	111.0	39.4	111.0
	1-8	8.2	2.5	32.8	10.0				
						25.0	5.0	25.0	5.0
	1-9	4.3	0	17.2	0				
						8.6	0	8.6	0
	1-10	0	0	0	0				
								137.2	227.6
#2	1-6	0	0	0	0				
						3.2	0	3.2	0
	1-7	1.6	0	6.4	0				
						7.0	4.6	7.0	4.6
	1-8	1.9	2.3	7.6	9.2				
						40.2	115.6	40.2	115.6
	1-9	18.2	55.5	72.8	222.0				
						71.0	168.6	71.0	168.6
	1-10	17.3	28.8	69.2	115.2				
						66.4	57.6	66.4	57.6
	1-11	15.9	0	63.6	0				
						40.8	0	40.8	0
	1-12	4.5	0	18.0	0				
						9.0	0	9.0	0
	1-13	0	0	0	0				
								237.6	346.4
#3	1-21	0	0	0	0				
						2.2	0	2.2	0
	1-22	1.1	0	4.4	0				
						4.8	20.6	4.8	20.6
	1-23	1.3	10.3	5.2	41.2				
						4.8	52.6	4.8	52.6
	1-24	1.1	16.0	4.4	64.0				
						6.4	54.4	6.4	54.4

*See page 71 for planimeter calibration.

TABLE A-III(continued)

	1-25a	2.1	11.2	8.4	44.8	4.2	22.4	4.2	22.4
	1-26a	0	0	0	0			22.4	150.0
#4	1-21	0	0	0	0				
	1-22	2.2	0	8.8	0	4.4	0	4.4	0
	1-23	2.2	0	8.8	0	8.8	0	8.8	0
	1-24	2.3	40.8	9.2	163.2	9.0	81.6	9.0	81.6
	1-25a	4.5	78.4	18.0	313.6	13.6	238.4	13.6	238.4
	1-26a	5.6	293.4	22.4	1173.6	20.20	743.6	20.2	743.6
	1-27a	33.2	146.3	132.8	585.2	77.6	879.4	77.6	879.4
	1-28a	69.3	22.8	277.2	91.2	205.0	338.2	205.0	338.2
	1-29	42.3	0	169.2	0	223.2	45.6	223.2	45.6
	1-30	15.5	0	62.0	0	115.6	0	115.6	0
	1-31	11.3	0	45.2	0	53.6	0	53.6	0
	1-32	7.8	0	31.2	0	38.2	0	38.2	0
	1-33	0	0	0	0	15.6	0	15.6	0
								784.8	2,326.8
#5	1-28a	0	0	0	0				
	1-29	9.1	0	36.4	0	18.2	0	18.2	0
	1-30	12.4	0	49.6	0	43.0	0	43.0	0
	1-31	16.8	0	67.2	0	58.4	0	58.4	0
	1-32	19.4	0	77.6	0	72.4	0	72.4	0
	1-33	17.1	24.9	68.4	99.6	73.0	49.8	73.0	49.8
	1-34	16.8	130.4	67.2	521.6	67.8	310.6	67.8	310.6
	1-35	18.0	160.0	72.0	640.0	69.6	580.8	69.6	580.8
						110.6	546.4	110.6	546.4

TABLE A-III(continued)

	1-36	37.3	113.2	149.2	452.8	107.6	295.8	107.6	295.8
	1-37	16.5	34.7	66.0	138.8	64.0	72.8	64.0	72.8
	1-38	15.5	1.7	62.0	6.8	37.2	3.4	37.2	3.4
	1-39	3.1	0	12.4	0	6.2	0	6.2	0
	1-40	0	0	0	0			728.0	1,859.6
#6	1-29	0	0	0	0	5.0	0	5.0	0
	1-30	2.5	0	10	0	7.0	0	7.0	0
	1-31	1.0	0	4.0	0	5.6	6.0	5.6	6.0
	1-32	1.8	3.0	7.2	12	3.6	27.8	3.6	27.8
	1-33	0	10.9	0	43.6	4.0	21.8	4.0	21.8
	1-34	2.0	0	8.0	0	4.0	0	4.0	0
	1-35	0	0	0	0			29.2	55.6
#7	2-3	0	0	0	0	0	1.8	0	1.8
	2-4	0	0.9	0	3.6	3.2	12.2	3.2	12.2
	2-5	1.6	5.2	6.4	20.8	3.2	10.4	3.2	10.4
	2-6	0	0	0	0	0	0	0	0
	2-7	0	0	0	0			6.4	24.4
#8	2'-2	0	0	0	0	7.0	3.0	7.0	3.0
	2'-3	3.5	1.5	14.0	6.0	64.0	38.6	64.0	38.6
	2'-4	28.5	17.8	114.0	71.2	85.6	216.4	85.6	216.4
	2'-5	14.3	90.4	57.2	361.6	80.2	685.8	80.2	685.8
	2'-6	25.8	252.5	103.2	1010.0	161.2	967.8	161.2	967.8

TABLE A-III(continued)

	2'-7	54.8	231.4	219.2	925.6	173.0	747.8	173.0	747.8
	2'-8	31.7	142.5	126.8	570.0	143.4	372.2	143.4	372.2
	2'-9	40.0	43.6	160.0	174.4	142.2	87.2	142.2	87.2
	2'-10	31.1	0	124.4	0	88.2	0	88.2	0
	2'-11	13.0	0	52.0	0	26.0	0	26.0	0
	2'-12	0	0	0	0			970.8	3,118.8
#9	2'-9	0	0	0	0	2.0	8.8	2.0	8.8
	2'-10	1.0	4.4	4.0	17.6	2.0	8.8	2.0	8.8
	2'-11	0	0	0	0			4.0	17.6
#10	2'-10	0	0	0	0	12.6	31.8	12.6	31.8
	2'-11	6.3	15.9	25.2	63.6	12.6	82.2	12.6	82.2
	2'-12	0	25.2	0	100.8	2.0	54.4	2.0	54.4
	2'-13	1.0	2.0	4.0	8.0	2.0	7.6	2.0	7.6
	2'-14	0	1.8	0	7.2	0	3.6	0	3.6
	2'-15	0	0	0	0			29.2	179.6
#11	2'-10	0	0	0	0	0	0.6	0	0.6
	2'-11	0	0.3	0	1.2	17.8	78.6	17.8	78.6
	2'-12	8.9	39.0	35.6	156.0	38.0	366.6	38.0	366.6
	2'-13	10.1	144.3	40.4	577.2	40.4	585.0	40.4	585.0
	2'-14	10.1	148.2	40.4	592.8	35.2	316.8	35.2	316.8
	2'-15	7.5	10.2	30.0	40.8	22.0	20.4	22.0	20.4
	2'-16	3.5	0	14.0	0	7.0	0	7.0	0
	2'-17	0	0	0	0			160.4	1,368.0

TABLE A-III(continued)

#12	2'-14	0	0	0	0			
	2'-15	7.7	30.1	30.8	120.4	15.4	60.2	15.4	60.2
	2'-16	3.8	162.5	15.2	650.0	23.0	385.2	23.0	385.2
	2'-17	20.2	162.3	80.8	649.2	43.0	649.6	43.0	649.6
	2'-18	32.2	88.4	128.8	353.6	104.8	501.4	104.8	501.4
	2'-19	33.7	17.8	134.8	71.2	131.8	212.4	131.8	212.4
	2'-20	43.3	0	173.2	0	154.0	35.6	154.0	35.6
	2'-21	29.1	0	116.4	0	144.8	0	144.8	0
	2'-22	15.3	0	61.2	0	88.8	0	88.8	0
	2'-23	2.5	0	10.0	0	35.6	0	35.6	0
	2'-24	0	0	0	0	5.0	0	5.0	0
								746.2	1,844.4
#13	2'-24	0	0	0	0				
	2'-25	0	1.6	0	6.4	0	3.2	0	3.2
	2'-26	0	17.6	0	70.4	0	38.4	0	38.4
	2'-27	0	35.0	0	140.0	0	105.2	0	105.2
	2'-28	7.7	86.3	30.8	345.2	15.4	242.6	15.4	242.6
	2'-29	27.3	186.6	109.2	746.4	70.0	545.8	70.0	545.8
	2'-30	51.3	275.7	205.2	1102.8	157.2	924.6	157.2	924.6
	2'-31	24.6	342.5	98.4	1370.0	151.8	1236.4	151.8	1236.4
	2'-32	24.6	357.3	98.4	1429.2	98.4	1399.6	98.4	1399.6
	2'-33	11.3	344.4	45.2	1377.6	71.8	1403.4	71.8	1403.4
	2'-34	9.3	349.4	37.2	1397.6	41.2	1387.6	41.2	1387.6
	2'-35	21.2	318.9	84.8	1275.6	61.0	1336.6	61.0	1336.6
	2'-36	17.3	282.5	69.2	1130.0	77.0	1202.8	77.0	1202.8
						62.8	1011.0	62.8	1011.0

TABLE A-III(continued)

	2'-37	14.1	223.0	56.4	892.0	39.0	818.0	39.0	818.0
	2'-38	5.4	186.0	21.6	744.0	22.2	682.0	22.2	682.0
	2'-39	5.7	155.0	22.8	620.0	20.8	564.4	20.8	564.4
	2'-40	4.7	127.2	18.8	508.8	29.2	464.8	29.2	464.8
	2'-41	9.9	105.2	39.6	420.8	19.8	210.4	19.8	210.4
								937.6	13576.8
#14	2-6	0	0	0	0	27.2	0	27.2	0
	2-7	13.6	0	54.4	0	63.8	0	63.8	0
	2-8	18.3	0	73.2	0	77.0	0	77.0	0
	2-9	20.2	0	80.8	0	65.4	118.0	65.4	118.0
	2-10	12.5	59.0	50.0	236.0	47.0	401.8	47.0	401.8
	2-11	11.0	141.9	44.0	567.6	45.4	394.0	45.4	394.0
	2-12	11.7	55.1	46.8	220.4	36.0	114.8	36.0	114.8
	2-13	6.3	2.3	25.2	9.2	12.6	4.6	12.6	4.6
	2-14	0	0	0	0			374.4	1,033.2

Calibration of Planimeter

a) For all proficorder traces the scales were:
   i) horizontal: 0.001 inches / division
   ii) vertical: 25 microinches / division
   Actual area = 10^{-3} x 25 x 10^{-6} = 2.5 x 10^{-8} in^2 / sq.

b) Planimeter units to traverse 20 squares on proficorder paper.
   i) 7 runs: 126, 126, 125, 125, 124, 126, 125
   ii) average: 877 / 7 x 20 = 6.26 units / sq.

c) Conversion scale for planimeter.
   Conversion factor = (2.5 x 10^{-8} $in.^2$ / sq.)/(6.26 units/sq.)
   Conversion factor = 4.0 x 10^{-9} $in.^2$ per planimeter unit

TABLE A-IV

DETERMINATION OF v_L AND K FOR THE 14 CAVITATION PITS TRACED

PSC*	Pit No.	D_P mils	D_P^3 mils^3	$v_R \times 10^3$ mils^3	$v_C \times 10^3$ mils^3	v_R/v_C	$v_L = v_C - v_R$ mils$^3 \times 10^3$	$K^{**} \times 10^3$
1	#6	1.1	1.331	29.2	55.6	.525	26.4	12.317
1	#9	1.1	1.331	4.0	17.6	.227	13.6	6.345
2	#7	1.35	2.461	6.4	24.4	.262	18.0	4.542
2	#3	1.95	7.416	22.4	150.0	.149	127.6	10.684
2	#1	2.1	9.261	137.2	227.6	.602	90.4	6.061
2	#10	2.1	9.261	29.2	179.6	.162	150.4	10.085
2	#2	2.7	19.683	237.6	346.4	.685	108.8	3.432
3	#5	4.2	74.088	728.0	1,859.6	.391	1,131.6	9.484
3	#4	4.3	79.507	784.8	2,326.8	.337	1,542.0	12.043
3	#11	4.75	107.174	160.4	1,368.0	.117	1,207.6	6.997
3	#12	4.85	114.086	746.2	1,844.4	.404	1,098.2	5.977
3	#14	5.0	125.000	374.4	1,033.2	.362	658.8	3.272
4	#8	6.7	300.763	970.8	3,118.8	.311	2,148.0	4.435
4	#13	10.3	1092.727	937.6	13,576.8	.069	12,639.2	7.182
						4.592		102.856

Average $v_R/v_C = 4.592 / 14 = 0.328$

Average $K = (102.856 / 14) \times 10^{-3} = 7.346 \times 10^{-3}$

*PSC means Pit Size Category

**$K = 0.621\ v_L/D_P^3$

TABLE A-V

PIT COUNT DATA FOR RMS & RMC CONSTANTS

PSC*	PIT SIZE RANGE** UNITS	MILS	NUMBER OF PITS ON POLISHED SURFACE*** #49	#50	#63	#64	#61	#68	#22	#23	TOTAL
1	1-2.5	0.46- 1.15	150	200	125	175	600	500	400	500	2650
2	2.5-4	1.15- 1.84	22	8	19	6	29	30	5	3	122
2	4-5	1.84- 2.30	2	2	4	2	8	9	1	2	30
2	5-6	2.30- 2.76	5	2	5	0	6	3	2	1	24
3	6-7	2.76- 3.22	3	2	6	3	5	4	0	0	23
3	7-8	3.22- 3.68	2	2	2	4	1	3	1	0	15
3	8-9	3.68- 4.14	0	0	4	6	2	2	1	0	15
3	9-10	4.14- 4.60	1	0	1	4	1	1	0	1	9
3	10-11	4.60- 5.06	1	0	5	1	3	1	0	0	11
3	11-12	5.06- 5.52	1	1	4	3	1	3	0	1	14
4	12-13	5.52- 5.98	1	0	1	1	2	1	0	0	6
4	13-14	5.98- 6.44	1	0	2	1	0	1	1	0	6
4	14-15	6.44- 6.90	0	0	1	2	2	0	0	0	5
4	15-16	6.90- 7.36	0	1	0	1	0	0	0	0	2
4	16-17	7.36- 7.82	0	0	0	1	0	0	0	0	1
4	17-18	7.82- 8.28	0	0	0	1	0	0	0	0	1
4	18-19	8.28- 8.74	0	0	0	0	0	0	0	0	0
4	19-20	8.74- 9.20	0	0	0	0	0	0	0	0	0
4	20-21	9.20- 9.66	0	0	0	0	1	0	0	0	1
4	21-22	9.66-10.12	0	0	0	0	0	0	0	0	0
4	22-23	10.12-10.58	0	0	1	0	0	0	0	0	0
4	23-24	10.58-11.04	0	0	0	0	0	0	0	0	0

*PSC means Pit Size Category

**One unit corresponds to one division on the scaled microscope eyepiece used to observe test samples.

***Samples 49, 50, 63, & 64 are stainless steel.
Samples 61 & 68 are carbon steel.
Samples 22 & 23 are columbium-1% zirconium.

TABLE A-VI

EXPANDED DATA FOR RMS & RMC CONSTANTS

PIT SIZE RANGE(mils)	n' PITS	$D_{P_{av}}$ mils	$D^2_{P_{av}}$ mils^2	$n'D^2_{P_{av}}$ mils^2	$D^3_{P_{av}}$ mils^3	$n'D^3_{P_{av}}$ mils^3
0.46- 1.15	2650	0.805	0.6480	1717.2000	0.5216	1382.2400
1.15- 1.84	122	1.495	2.2350	272.6700	3.3413	407.6386
1.84- 2.30	30	2.07	4.2849	128.5470	8.8697	266.0910
2.30- 2.76	24	2.53	6.4009	153.6216	16.1943	388.6632
	176			554.8386		1062.3928
2.76- 3.22	23	2.99	8.9401	205.6223	26.7309	614.8107
3.22- 3.68	15	3.45	11.9025	178.5375	41.0636	615.9540
3.68- 4.14	15	3.91	15.2881	229.3215	59.7765	896.6475
4.14- 4.60	9	4.37	19.0969	171.8721	83.4535	751.0815
4.60- 5.06	11	4.83	23.3289	256.6179	112.6786	1239.4646
5.06- 5.52	14	5.29	27.9841	391.7774	148.0359	2072.5026
	87			1433.7487		6190.4609
5.52- 5.98	6	5.75	33.0625	198.3750	190.1094	1140.6564
5.98- 6.44	6	6.21	38.5641	231.3846	239.4831	1436.8986
6.44- 6.90	5	6.67	44.4889	222.4445	296.7410	1483.7050
6.90- 7.36	2	7.13	50.8369	101.6738	362.4671	724.9342
7.36- 7.82	1	7.59	57.6081	57.6081	437.2455	437.2455
7.82- 8.28	1	8.05	64.8025	64.8025	521.6601	521.6601
8.28- 8.74	0	8.51	72.4201	0	616.2951	0
8.74- 9.20	0	8.97	80.4609	0	721.7343	0
9.20- 9.66	1	9.43	88.9249	88.9249	838.5618	838.5618
9.66-10.12	0	9.89	97.8121	0	967.3617	0
10.12-10.58	1	10.35	107.1225	107.1225	1108.7179	1108.7179
10.58-11.04	0	10.81	116.8561	0	1263.2144	0
	23			1072.3359		7692.3795

TABLE A-VII

DETERMINATION OF RMS & RMC CONSTANTS

PSC*	$\sum n_i'$	$\sum n_i' D_{P_{av_i}}^2$	$\sum n_i' D_{P_{av_i}}^3$	S_i	D_{RMS_i}	C_i	D_{RMC_i}
1	2650	1717.2000	1382.2400	0.6480	0.805	0.5216	0.805
2	176	554.8386	1062.3928	3.1525	1.776	6.0363	1.821
3	87	1433.7487	6190.4609	16.4799	4.060	71.1547	4.144
4	23	1072.3359	7692.3795	46.6233	6.828	334.4513	6.941

The RMS and RMC constants are defined as follows (where i corresponds to the pit size categories 1,2,3,4):

$$C_i = \sum(n' D_{P_{av}}^3)_i \; / \; \sum n_i'$$

$$D_{RMC_i} = C_i^{.333}$$

$$S_i = \sum(n_i' D_{P_{av}}^2)_i \; / \; \sum n_i'$$

$$D_{RMS_i} = S_i^{.500}$$

*PSC means Pit Size Category.

TABLE A-VIII

PIT COUNT DATA TO DETERMINE K_S^*

PIT SIZE CATEGORY	FLUID	SAMPLE NUMBER	NUMBER OF PITS SURFACE	SIDES	SIDES/SURFACE	k_{S_i}
1	Hg	SS- 78	800	2300		
		SS-112	400	1600		
		Total	1200	3900	3.250	
	H_2O	SS- 4	400	790		
		SS- 5	480	670		
		Total	880	1460	1.659	2.454
2	Hg	SS- 63	73	260		
		SS- 64	94	330		
		Total	167	590	3.532	
	H_2O	SS- 4	75	136		
		SS- 5	110	112		
		Total	185	248	1.340	2.436
3	Hg	SS- 63	31	85		
		SS- 64	29	71		
		Total	60	156	2.600	
	H_2O	SS- 4	17	67		
		SS- 5	18	33		
		Total	35	100	2.857	2.728
4	Hg	SS- 63	27	35		
		SS- 64	26	76		
		Total	53	111	2.094	
	H_2O	SS- 4	10	39		
		SS- 5	13	41		
		Total	23	80	3.478	2.786

$$k_S = (2.454 + 2.436 + 2.728 + 2.786)/ 4 = 2.601$$

$$K_S = k_S + 1 = 2.601 + 1.000$$

$$K_S = 3.601$$

---

*Test durations: SS 78 & 112-10 hrs.; SS 63 & 64-100 hrs.; SS 3 & 4-150 hrs.